

**EFFECT OF INTERFACE CRACK AND CORNER  
SINGULARITY IN BIMATERIAL SYSTEM –  
EXPERIMENTAL AND NUMERICAL  
INVESTIGATION**

*Dissertation submitted in partial fulfillment of the requirements for the  
award of the degree of*

*Master of Technology*

Submitted by

**Rahul N Pai**  
(ME10M08)

With the guidance of

**Dr. M Ramji**

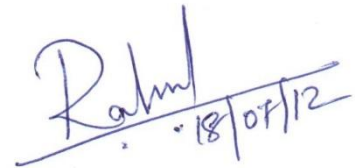


भारतीय प्रौद्योगिकी संस्थान हैदराबाद  
Indian Institute of Technology Hyderabad

**Department of Mechanical Engineering  
Indian Institute of Technology Hyderabad  
July, 2012**

## **DECLARATION**

I declare that this written submission represents my ideas in my own words, and where others' ideas or words have been included, I have adequately cited and referenced the original sources. I also declare that I have adhered to all principles of academic honesty and integrity and have not misrepresented, fabricated or falsified any idea/data/fact/source in my submission. I understand that any violation of the above will be a cause for disciplinary action by the Institute and can also evoke penal action from the sources that have thus not been properly cited, or from whom proper permission has not been taken when needed.

A handwritten signature in blue ink that reads "Rahul" followed by a horizontal line and the date "18/07/12".

(Signature)

**Rahul N Pai**

(Student Name)

**ME10M08**

(Roll No.)

## APPROVAL SHEET

This thesis entitled "*Effect of Interface Crack and Corner Singularity in Bimaterial System – Experimental and Numerical Investigation*" by **Rahul N Pai** is approved for the degree of **Master of Technology** from IIT Hyderabad.

M. M. 16/07/12

Dr. M. Ramji, Asst. Professor, IIT Hyderabad  
Adviser

v. Chandrika

Dr. Chandrika Prakash Vyasarayani, Asst. Professor, IIT Hyderabad  
Examiner

Manoj Pandey

Dr. Manoj Pandey, Asst. Professor, IIT Hyderabad  
Examiner

Umashankar

Dr. B. Umashankar, Asst. Professor, IIT Hyderabad  
Chairman

## **ACKNOWLEDGEMENTS**

One walks alone on the journey of life. Just where you start to thank those that joined you, walked beside you, and helped you along the way. First and foremost, I would like to express a deep sense of gratitude towards my guide Dr. M Ramji for the valuable guidance and advice. He inspired me greatly to work in this project. His willingness to motivate me contributed tremendously to this project. I thank my parents for their constant support. I take immense pleasure in thanking Mr. R G R Prasad for his great support in doing the experiments and its post processing. I would like to thank workshop staffs, Mr. A. Praveen Kumar and Mr. S. Jagadeesan for their help in preparing the samples for the study. I would like to thank Ph.D. student, Mr. Mohammad Kashfuddoja for helping and giving suggestions on finite element modeling aspects. Last but not least, I would like to thank the institute, mechanical engineering department, and head of the department. I would also like to thank all my classmates for their valuable suggestions and helpful discussions. Once again I would like to thank all the people who helped me for the successful completion of my work.

***\* DEDICATED TO MY PARENTS \****

## **ABSTRACT**

It is of great importance to study behavior of adhesively bonded dissimilar materials as they are widely used in electronic packaging, plastic integrated circuit, welded joints of dissimilar materials, composite materials etc. Due to mechanical loading, cyclic variation in climate or changes in moisture content of ambience leads to high stress at corners or interface, where discontinuities of geometry or material property is present. In this study an attempt has been made to study the behavior of small crack at the interface of aluminum/epoxy bimaterial system. Initially stress intensity factors are estimated experimentally by digital photoelasticity and then compared numerically with a finite element model. Experimentally, ten-step phase shifting technique is used to get isochromatic phase map without ambiguity and later it is unwrapped to get the total fringe order over the model domain. Three fringe photoelasticity technique is also used to get total fringe order. From this information stress intensity factor at interface crack tip is determined using simplified multi-parameter stress field equation of Deng involving over-deterministic least square approach. Numerically stress intensity factors are evaluated by virtual crack closure integral method. Numerically  $J$ -integral method is also used for evaluating stress intensity factors for interface crack. We may have to account for the effect of material mismatch as well as temperature effect at material interfaces. A bimaterial wedge corner can also act as a source for high stress concentration, and its singularity is different from crack tip. In the present work, analytically order of singularity is found out for the aluminium/epoxy bimaterial system and using this, stress fields around the corner is predicted. For finding the order of singularity modified stress field equations of Seweryn has been used with appropriate boundary conditions. A linear elastic fracture mechanics frame work is applied for the entire study.

# Contents

## Chapter 1 Introduction and Literature Review

<b>1.1</b> Introduction .....	<b>1</b>
<b>1.1.1</b> Introduction to fracture mechanics of bimaterial system .....	<b>2</b>
<b>1.1.2</b> Introduction to digital photoelasticity applied to bimaterial fracture.....	<b>4</b>
<b>1.1.3</b> Finite element method applied to bimaterial fracture.....	<b>7</b>
<b>1.2</b> Scope and motivation .....	<b>8</b>
<b>1.3</b> Thesis layout .....	<b>9</b>

## Chapter 2 Experimental and Numerical Evaluation of SIF for a Bimaterial Interface Crack

<b>2.1</b> Introduction .....	<b>10</b>
<b>2.2</b> Stress field equations for an interfacial crack .....	<b>12</b>
<b>2.3</b> Experimental analysis .....	<b>14</b>
<b>2.3.1</b> Specimen preparation .....	<b>14</b>
<b>2.3.2</b> Total fringe order evaluation .....	<b>15</b>
<b>2.3.3</b> Photoelastic determination of SIF .....	<b>18</b>
<b>2.4</b> Numerical evaluation of SIF .....	<b>19</b>
<b>2.4.1</b> VCCI technique .....	<b>20</b>
<b>2.4.2</b> Finite element modeling of bimaterial .....	<b>21</b>
<b>2.5</b> Results and discussions .....	<b>23</b>
<b>2.6</b> Closure .....	<b>27</b>

## Chapter 3 Experimental and Numerical Evaluation of Order of Singularity

<b>3.1</b> Introduction .....	<b>28</b>
<b>3.2</b> Stress field equations for an interfacial corner .....	<b>30</b>
<b>3.3</b> Analytical determination of order of singularity .....	<b>30</b>
<b>3.4</b> Experimental analysis .....	<b>32</b>
<b>3.4.1</b> Specimen preparation .....	<b>32</b>
<b>3.4.2</b> Total fringe order estimation .....	<b>32</b>

<b>3.5</b> Finite element modeling of bimaterial .....	<b>33</b>
<b>3.6</b> Results and discussions .....	<b>34</b>
<b>3.7</b> Closure .....	<b>43</b>
<b>Chapter 4</b> Conclusions and Future Recommendations .....	<b>44</b>
Appendix <b>A</b> Ten-step Images Grabbed for Linear Configuration .....	<b>45</b>
Appendix <b>B</b> Deriving of SIF for an Interfacial Crack .....	<b>46</b>
References .....	<b>48</b>
List of Papers Published on the Basis of this Thesis .....	<b>51</b>



# List of Figures

Figure <b>1.1</b> : Application of adhesively bonded dissimilar materials (a) Sectional view of a single silicon chip (b) Application of TSV technology .....	<b>2</b>
Figure <b>1.2</b> : Dark field plane polariscope image of a disk under diametric compression showing both isoclinic and isochromatic fringe contours .....	<b>4</b>
Figure <b>1.3</b> : Generic arrangement for a circular polariscope set up .....	<b>5</b>
Figure <b>1.4</b> : General procedure in digital photoelasticity for isochromatic parameter estimation (a) Isochromatic phasemap (b) Unwrapped isochromatic phasemap (c) Unwrapped isochromatic phasemap (3-D plot) .....	<b>6</b>
Figure <b>2.1</b> : Bimaterial configurations used for study (a) Linear configuration (b) Stack configuration .....	<b>11</b>
Figure <b>2.2</b> : Co-ordinate system for interfacial crack .....	<b>12</b>
Figure <b>2.3</b> : Bimaterial specimens used for experimental analysis (a) Linear configuration (b) Stack configuration (c) Zoomed view of crack tip .....	<b>15</b>
Figure <b>2.4</b> : Dark field color image of bimaterial specimen at 125 N (a) full isochromatic view subjected to four point bending (b) Zoomed part near the crack tip .....	<b>17</b>
Figure <b>2.5</b> : Dark field colour image of bimaterial specimen at 250 N (a) Full isochromatic view (b) Zoomed part near the crack tip .....	<b>19</b>
Figure <b>2.6</b> : Coordinate system for bimaterial crack .....	<b>20</b>
Figure <b>2.7</b> : FE model of bimaterial specimen (linear configuration) (a) Complete meshed model (b) Zoomed part near crack tip .....	<b>22</b>
Figure <b>2.8</b> : FE model of bimaterial specimen (stack configuration) (a) Complete meshed model (b) Zoomed part near crack tip .....	<b>22</b>
Figure <b>2.9</b> : FE model of bimaterial specimen (linear configuration) (a) Complete meshed model (b) Zoomed part near crack tip .....	<b>22</b>
Figure <b>2.10</b> : FE model of bimaterial specimen (stack configuration) (a) Complete meshed model (b) Zoomed part near crack tip .....	<b>23</b>
Figure <b>2.11</b> : Experimental data from photoelasticity using ten-step method (a) Wrapped isoclinic phase map (b) Unwrapped isoclinic phase map (c) Isochromatic phase map (d) Grey scale plot for unwrapped isochromatic phase map (e) MATLAB plot .....	<b>24</b>

Figure 2.12: Theoretically reconstructed isochromatic fringe patterns (dark field and bright field) with data points superimposed for (a) One parameter (b) Two parameter (c) Three parameter (d) Four parameter .....	25
Figure 2.13: Total fringe order plot for stack configuration using TFP (a) Gray scale plot (b) 3D plot of total fringe order .....	26
Figure 2.14: Theoretically reconstructed isochromatic fringe patterns with data points superimposed for six parameter (a) Dark field (b) Bright field .....	26
Figure 3.1: Bimaterial configurations used for study (a) Linear configuration (b) Stack configuration .....	29
Figure 3.2: Coordinate system for bimaterial wedge problem .....	30
Figure 3.3: Bimaterial specimens used for experimental analysis (a) Linear configuration (b) Stack configuration .....	32
Figure 3.4: Dark field image taken at 150 N for linear configuration (a) Full dark field (b) Zoomed part near the corner .....	33
Figure 3.5: Dark field image taken at 300 N for stack configuration (a) Full dark field (b) Zoomed part near the corner .....	33
Figure 3.6: FE model of bimaterial specimen having linear configuration (a) Full meshed model (b) Zoomed part near corner .....	34
Figure 3.7: FE model of bimaterial specimen having stack configuration (a) Full meshed model (b) Zoomed part near corner .....	34
Figure 3.8: Eigen value determination for linear configuration (a) Co-ordinate system for linear configuration (b) Graph showing obtained value of singularity .....	35
Figure 3.9: Eigen value determination for stack configuration (a) Co-ordinate system for stack configuration (b) Graph showing obtained value of singularity .....	36
Figure 3.10: Total fringe order plot for linear configuration (a) Gray scale plot for total fringe order (b) 3D plot for total fringe order .....	36
Figure 3.11: Total fringe order plot for stack configuration (a) Gray scale plot for total fringe order (b) 3D plot for total fringe order .....	37

# List of Tables

Table 2.1: Material properties .....	11
Table 2.2: Optical arrangements of ten-step method .....	17
Table 2.3: Comparison of SIF .....	27
Table 3.1: $H$ value for different bimaterial configurations .....	42

# Chapter 1

## Introduction and Literature Review

### 1.1 Introduction

A plastic integrated circuit (IC) is a complex mixture of different classes of materials. It may contain ceramics such as silicon for the die, organics such as epoxy for molding compounds and substrates, and metals for lead frames etc. These materials have different mechanical and thermal properties from one another. So in electronic packaging a care should be given for multi-material interfaces as these are the potential sites for delamination due to great difference in material properties. Thermal loads due to climatic changes and operating conditions of the electronic device may introduce thermal stress in the materials and each material will behave according to its thermal properties. Studies have shown that huge stress can occur in interface of these materials where drastic changes in material properties as well as geometric irregularities are present [1, 2]. In real life situation one may find many combinations of dissimilar materials in welded joints, thermostats, composites etc. So it is of great importance to understand the interface behavior of adhesively bonded dissimilar materials.

Focusing on integrated circuits, they are used virtually in all electronic equipments today and have revolutionized the way it is being constructed. Computers, mobile phones and other digital home appliances are now inextricable parts of the structure of modern societies, made possible by the low cost of production of integrated circuits. The integration of large numbers of tiny transistors into a small chip has been an enormous improvement over the manual assembly of circuits using discrete electronic components. The integrated circuits mass production capability, reliability, and building-block approach to circuit design ensured the rapid adoption of standardized integrated circuits in place of designs using discrete transistors. Figure 1.1a shows sectional view of a single silicon chip adhesively bonded over plastic case, which may be organics such as epoxy. For electrical connectivity copper lead wires are pasted in the plastic case, which intern is in contact with silicon chip. So even in a single chip one can find adhesive bonding of dissimilar materials and it has to be given great care during its operation. Through silicon via (TSV) is the latest in a progression of technologies for stacking silicon devices in three dimensions (3D). Driven by the need

for improved performance, methods to use short vertical interconnects to replace the long interconnects found in 2D structures have been developed. Figure 1.1b shows TSV technology adopted in electronic packaging, where we can connect large number of single chips in 3D. TSV therefore refer to a 3D package that contains two or more integrated circuits stacked vertically so that they occupy less space on a printed circuit board (PCB). TSV replace edge wiring by creating vertical connections through the body of the chips. The resulting package has no added length or width. Because no interposer is required, a TSV 3D package can also be flatter than an edge-wired 3D package. This TSV technique is sometimes also referred to as through-silicon stacking (or thru-silicon stacking, TSS).

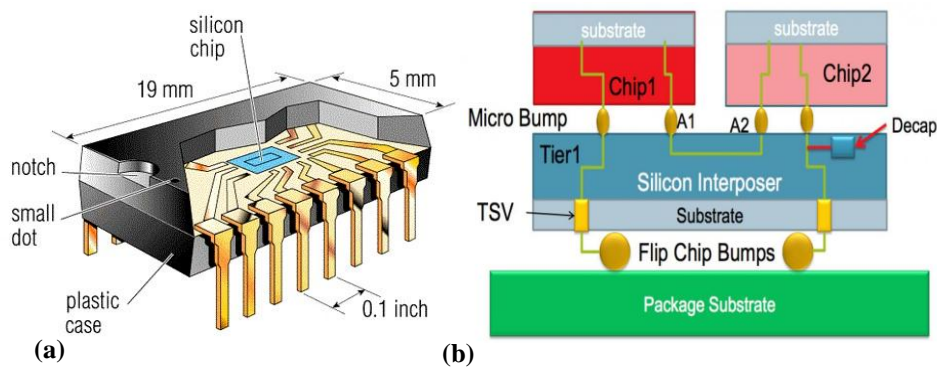


**Figure 1.1: Application of adhesively bonded dissimilar materials [3] (a) Sectional view of a single silicon chip (b) Application of TSV technology**

### 1.1.1 Introduction to fracture mechanics of bimaterial system

Fracture mechanics is a branch of engineering which deals with the study of failures in engineering structures. It works on the assumption that all the engineering structures are associated with inbuilt flaws (cracks, voids, impurities, inclusions etc.). These flaws play an important role in the failure of the structures. According to fracture mechanics a member can fail due to three modes of failures, mode I, mode II, mode III or a combination of these. Mode I failure is associated with opening mode failure wherein the displacement will occur normal to the crack plane. Mode II failure is associated with shear mode failure where in the displacement will occur parallel to the crack plane. Mode III failure is associated with tearing mode failure wherein displacement will occur parallel to the crack front. Each mode stress field is quantized by a parameter called stress intensity factor (SIF) and they characterize the stress field surrounding the crack tip. Associated with three modes, we have three SIF's,  $K_I$ ,  $K_{II}$ , and  $K_{III}$  for mode I, mode

II and mode III respectively. The plane problem of a crack lying along the interface of two dissimilar media in linear elasticity is one of great importance. Williams [4] in 1959 formulated a bimaterial interface crack problem using the eigen function approach. He considered only the first eigenvalue in the sets of solution obtained and observed an oscillatory behavior of the stresses when the crack tip is approached. He also observed that the oscillatory behavior of the stresses is confined quite close to the base of the crack. This does not arise in reality, as the crack tip cannot occupy two different materials at the same time. In the case of homogeneous medium, the stress field near the crack tip could be identified separately for mode-I and mode-II. In the case of an interface crack in bimaterial joint, the tensile and shear effects near the crack tip are inseparable and SIF is usually expressed as a complex number. Various definitions of SIF are reported in the literature, the basic definitions of SIF has units  $\text{MPa m}^{1/2} \text{ m}^{-i\epsilon}$  ( $\epsilon$ -bimaterial constant), which is inconvenient to use in experimental studies.

For the problem of cracks in homogeneous solids, it is well documented that the use of singular solution to model the near-tip stress field is inadequate. The use of a multi-parameter solution to evaluate the SIF is well established [5]. Unlike the situation for the homogeneous case, in a bimaterial interface crack problem, the need for higher-order terms has not been felt in earlier days. In 1988, Rice [6] gave the form of series solution that includes integer order terms. In 1993, Deng [7] reported another form of stress field equations in cartesian coordinates. Although the form of equations given by Deng is simpler than that stated by Rice, still it is not in a form that could be directly used for numerical computations. Ravichandran and Ramesh [8] have simplified the stress field equations of Deng suitable for experimental study.

Studies have found that bimaterial corners (wedges) will give rise to stress concentrations and are almost similar to a crack. So a care should be given to angular corners in dissimilar materials. Generally stress fields near the corner of bimaterial are expressed as (Eq. 1.1),

$$\sigma_{ij} = \frac{k}{r^{\lambda-1}} \quad (1.1)$$

where,  $k$  is corner SIF and  $\lambda$  will give order of singularity. In the case of homogeneous material order of singularity is 0.5 while in the case of dissimilar material corner, order of singularity can vary between (0, 1). Also  $\lambda$  value will depend on the material properties and wedge angle and is independent of type of loading.

### 1.1.2 Introduction to digital photoelasticity applied to bimaterial fracture

There are many experimental techniques available for SIF estimation such as Moiré, Holography, Digital Image Correlation (DIC) and Photoelasticity. In the present work photoelasticity is used for SIF estimation [9]. Photoelasticity is an optical non-contact technique for whole field stress analysis which provides the information of principal stress difference (isochromatics) and principal stress direction (isoclinics) in the form of fringe contour (see Figure 1.2). This is the only technique which can analyze the interior of 3-D models. Figure 1.3 shows generic arrangement for a circular polariscope set up.

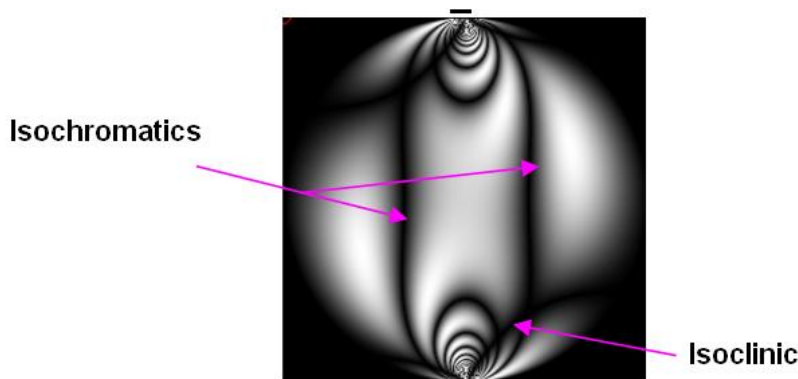


**Figure 1.2: Dark field plane polariscope image of a disk under diametric compression showing both isoclinic and isochromatic fringe contours [10]**

With the advent of computer based digital image processing systems, automation of photoelastic parameter estimation has now become possible. Voloshin and Burger [11] were the first to exploit the intensity data and developed half fringe photoelasticity (HFP). It can give fringe order in the range (0, 0.5). A paradigm shift in data acquisition methodologies came into existence with the development of charge coupled device (CCD) cameras which could record intensity data at video rates. Afterwards several whole field techniques came into existence. The techniques could be broadly classified into spatial domain and frequency domain methods. Phase shifting techniques (PST), polarization stepping techniques and load stepping come under spatial domain methods. Fourier transform approach comes under frequency domain method. The frequency domain methods usually demand more images to be recorded (even 90 images in some cases) and are computationally very intensive. On the other hand spatial domain methods require smaller number of images to be recorded (from three to ten in most cases). Further, they are computationally very fast and rugged therefore they are considered in this work for whole field parameter estimation.

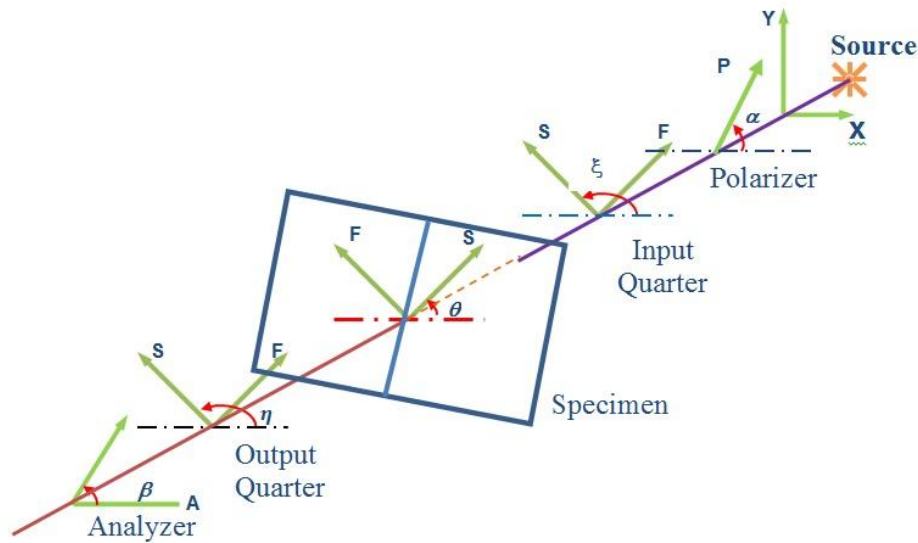


**Figure 1.3: Generic arrangement for a circular polariscope set up**

The phase shifting algorithms basically provide isochromatic values in the form of wrapped phasemaps which are different from the conventional fringe patterns of photoelasticity (Figure 1.4a). The wrapped phasemap essentially gives the fractional retardation at the point of interest. Unwrapping of isochromatic phasemap refers to the suitable addition of integral value to the fractional retardation values for making it as a continuous phase data. One of the simplest approaches for unwrapping of isochromatic phasemap is by raster scanning approach [12]. The unwrapped isochromatic phasemap is shown in Fig. 1.4b and 3-D view of the unwrapped isochromatic phasemap is shown in Fig. 1.4c. Raster scanning approach is not autonomous and becomes very tedious while handling domains of complicated geometries. Presently, use of quality guided approach [13] for phase unwrapping that has been developed in other optical techniques has gained prominence in photoelasticity because of its autonomous capability.

For whole field parameter estimation, colour matching techniques were also used, wherein one can process the colour images and get the data out of it. Three fringe photoelasticity (TFP) [14] can give total fringe order from a single colour isochromatic fringe field by suitably comparing the colour with calibration specimen. The colours tend to merge beyond third fringe order and hence the technique is termed as TFP. Discontinuities in fringe order variation are smoothed using the refined TFP (RTFP) procedure [15].



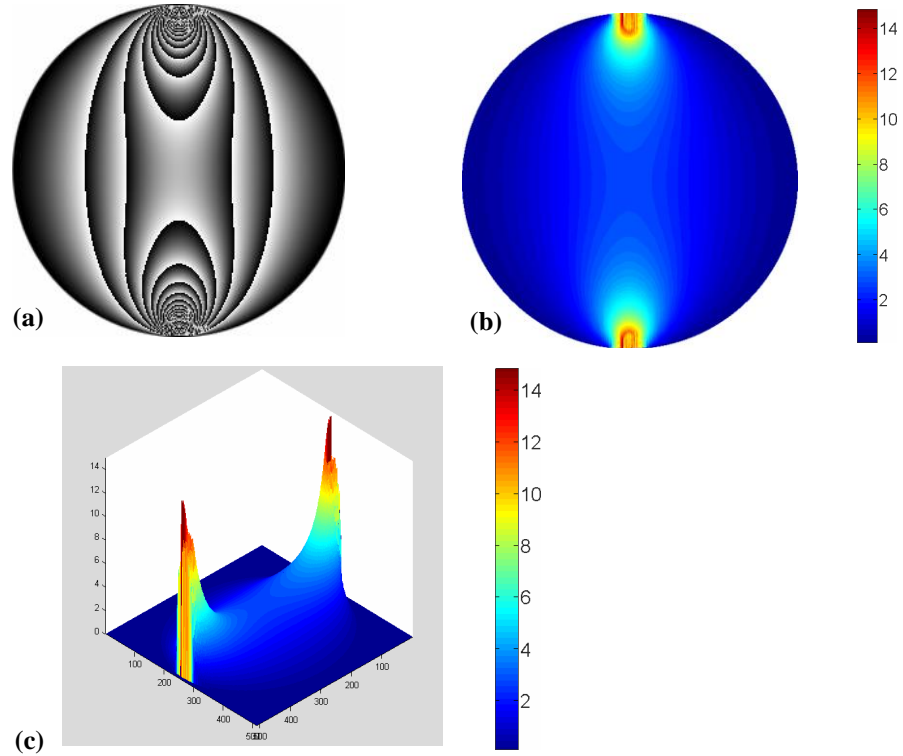


**Figure 1.4: General procedure in digital photoelasticity for isochromatic parameter estimation (a) Isochromatic phasemap (b) Unwrapped isochromatic phasemap (c) Unwrapped isochromatic phasemap (3-D plot)**

In 1993, Lu and Chiang [16] used singular stress field equation with two point approach for evaluation of complex SIF in a bimaterial model. In 1999, Soh [17] used least squares approach by taking large number of data points surrounding the crack tip. Although this technique uses the full field information of photoelastic fringes, the governing equation is still the singular stress field equation. For a crack in homogeneous material use of multi-parameter solution to evaluate SIF is well established. For bimaterial problems, Deng [7] reported a set of stress field equations in cartesian coordinates which are simpler than the field equations of Rice [6]. Later, Deng equations were modified by Ravichandran and Ramesh [8] making it suitable for digital photoelastic technique.

In the present study, first, the total fringe order is obtained at each pixel over the entire model domain by employing either, ten-step phase shifting technique [18] or RTFP [15] depending upon the problem. Then, this fringe order ( $N$ ) and the coordinates ( $r, \theta$ ) defining the location of  $m$  different points of interest near the crack front are used for evaluating the mixed-mode stress field parameters using the stress field equations of Deng (modified) with the help of an over-deterministic least square

approach. The software based on the digital image processing techniques is utilized for the required automatic data collection, thus, avoiding any human error. Then, the experimental fringes are remodeled using the evaluated stress field parameters. The number of the terms in mode I and mode II expression are increased independently till the experimental fringes coincides with the reconstructed fringe patterns obtained using estimated parameters.

In literature, stress fields around the interface crack in dissimilar materials are characterized by different researchers [19-21]. Later on people have found that stress field around interface wedges (corners) of dissimilar materials play an important role in interfacial delamination. Stress field around these corners can act as source of stress concentration and may open up the interface. But unlike homogeneous material order of singularity for a bimaterial corner will depend on the value of  $\lambda$ , and in general stress field around the interface edge is expressed as a function of  $r^{\lambda-1}$ . The value of order of singularity will be in the interval (0,1). There has been many experimental and theoretical investigations on the stress distribution of ceramic-metal joints [19-21]. Moirè interferometry is one of the popularly used experimental technique for getting displacement field around the joints. In 2005, Liton kumar *et al.* [22] used this technique for capturing the singular fields around an interface edge of ceramic-metal joint.

Analytical studies for finding the order of singularity for a homogeneous material wedge has been done in 1996 by Seweryn [23]. In 2005, Yaping Luo and Ganesh Subbarayan [24] have extended the previous work for dissimilar materials and they estimated corner SIF involving FEA. In the present work the procedure for finding  $\lambda$  value for Aluminum/Epoxy bimaterial models is done by same approach and stress field (maximum shear stress) has been plotted around the bimaterial corner by both experimental and numerical method. Digital photoelasticity is used for finding the maximum shear stress distribution around the corner of bimaterial and it has been validated by finite element method (FEM).

### **1.1.3 Finite element method applied to bimaterial fracture**

The FEM (its practical application often known as finite element analysis (FEA)) is a numerical technique for finding approximate solutions of partial differential equations (PDE) as well as integral equations. The solution approach is based either on eliminating the differential equation completely (steady state problems), or rendering

the PDE into an approximating system of ordinary differential equations, which are then numerically integrated using standard techniques such as Euler's method, Runge-Kutta, etc.

There are many techniques to evaluate SIF such as compounding method, displacement extrapolation method, force method,  $J$ -integral, singularity subtraction technique and virtual crack closure method (VCCT) in its classical and modified form. Numerical estimation of SIF for an interfacial crack can be done by exploiting Irwin's theory, the work required to extend a crack by an infinitesimal distance is equal to the work required to close the crack to its original length. The study is particularly important as the fracture at or near the interfaces is critical leading to different failure modes in composites including debonding and delamination. In 1994, Dattaguru et al. [25] used modified crack closure integral (MCCI) technique to estimate the energy release rates of bimaterial interface crack problems. In this work, SIF's are evaluated numerically by virtual crack closure integral (VCCI) method [26]. This method will compute the mixed mode SIF's from mixed mode energy release rates of the interfacial crack which are obtained from crack tip opening displacements and the nodal forces at and ahead of the crack tip in FE model. SIF is evaluated from FE model by implementing VCCI technique. In the present study we have also evaluated bimaterial SIF by applying  $J$ -integral approach. Finally experimental results are compared with FE results.

## 1.2 Scope and Motivation

Interface problem play an important role in microelectronic interconnect structures. The interconnect structure is very complex and involves many interfaces between dissimilar materials. Since there is material mismatch at the interface, temperature gradient would play an important role in it's the stress fields around the interface. There are very few works involved with the experimental characterisation of crack tip as well as corner singularity associated with bimaterial system. There are many studies showing the effect of temperature on bimaterial interfaces, and it will become more useful for studying microelectronic structures. It is found that most of the studies has been done uising FEM, and very few experimental characterization exists in literature. Researchers have attempted this problem experimentally using Moirè interferometry and very few commented using digital photoelasticity. In this present work an attempt

has been made to characterize the stress fields near the interface crack as well as corner singularity for an Aluminum/Epoxy bimaterial model involving digital photoelasticity.

### **1.3 Thesis Layout**

Chapter 1 deals with introduction to multi-material interface mechanics as well as literature review.

Chapter 2 deals with experimental and numerical evaluation of SIF for Al / Epoxy bimaterial interface crack subjected to pure bending.

Chapter 3 deals with experimental and numerical evaluation of order of singularity at the corner of Al / Epoxy bimaterial subjected to pure bending.

Chapter 4 deals with the future work and recommendations.

# Chapter 2

## Experimental and Numerical Evaluation of SIF for a Bimaterial Interface Crack

### 2.1 Introduction

Interfacial fracture mechanics has become an important area as there exist wide applications in the field of electronic packaging. As mentioned in the previous chapter a single electronic chip has been made with different interconnects which forms different interfaces of dissimilar materials. These interconnects play an important role in the failure of the chip due to difference in the mechanical properties of the materials joining the interface as well as its geometry. So a great care has to be given to the interface as it is a potential site for delamination to occur. Delamination starts in an interface when it is having faults like voids, impurities or inclusions etc., which in turn forms a crack. Crack can propagate because of thermal loads due to climatic changes or mechanical loads coming on the model. In the present study a small crack is made on the interface of Al/Epoxy bimaterial subjected to four point bending load and SIF is evaluated by digital photoelasticity. And this has been validated by FEM.

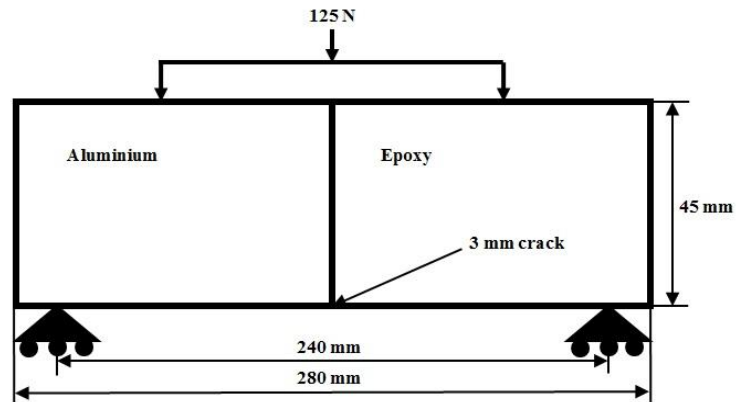
As discussed in chapter 1, TSV technique mainly uses linear configuration or stack configuration for manufacturing the interconnects. So in the present study linear as well as stack configuration is preferred for the analysis. The dimensions of these bimaterial configurations are given in figure 2.1. First configuration (linear configuration) is having 3 mm crack while second configuration (stack configuration) is having 19 mm crack along the interface and both materials are having a thickness of 6 mm in transverse direction. Analysis is carried out at 125 N for linear configuration while at 250 N for stack configuration. In the present work we have employed linear fracture mechanics approach and plain strain condition is assumed. The specimens are loaded mechanically under four point bending. Table 2.1 shows the material properties of aluminum and epoxy.

In this chapter, SIF deduction for above mentioned configurations is done by digital photoelasticity as well as FEM. In experimental part, discussion on specimen preparation, experimental set up, stress field equations for bimaterial, total fringe order estimation, data collection and SIF deduction using least squares techniques is carried

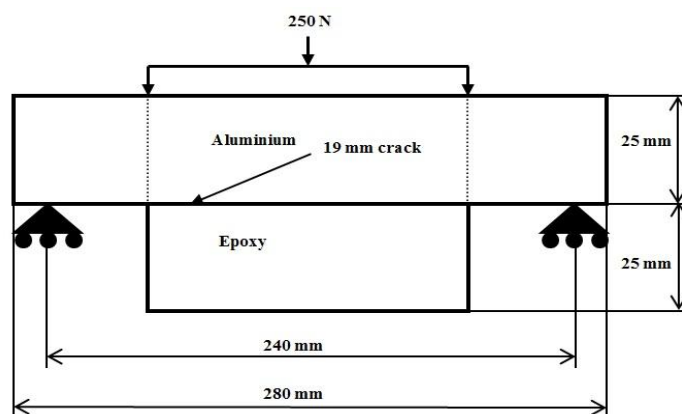
out. In numerical part, VCCI technique is employed to evaluate SIF for bimaterial interface crack. Finally results obtained from digital photoelasticity and FEM are compared.

Table 2.1: Material properties

Properties	Aluminum	Epoxy
Young's modulus, $E$	70 GPa	3.5 GPa
Poisson's ratio, $\nu$	0.33	0.35
Material stress fringe value, $F_\sigma$	----	10.5 N/mm fringe



(a)



(b)

Figure 2.1: Bimaterial configurations used for study (a) Linear configuration  
(b) Stack configuration

## 2.2 Stress field equations for an interfacial crack

The plane problem of a crack lying along the interface of two dissimilar media in linear elasticity is one of great importance. Williams [4] in 1959 formulated a bimaterial interface crack problem using the eigen function approach. He considered only the first eigenvalue in the sets of solution obtained and observed an oscillatory behaviour of the stresses when the crack tip is approached. He also observed that the oscillatory behaviour of the stresses is confined quite close to the base of the crack. This does not arise in reality, as the crack tip cannot occupy two different materials at the same time. In the case of homogeneous medium, the stress field near the crack tip could be identified separately for mode-I and mode-II. In the case of an interface crack in bimaterial joint, the tensile and shear effects near the crack tip are inseparable and SIF is usually expressed as a complex number. Various definitions of SIF are reported in the literature, the basic definitions of SIF has units  $\text{MPa m}^{1/2} \text{ m}^{-i\epsilon}$  ( $\epsilon$ - bimaterial constant), which is inconvenient to use in experimental studies.

For the problem of cracks in homogeneous solids, it is well documented that the use of singular solution to model the near-tip stress field is inadequate. The use of a multi-parameter solution to evaluate the SIF is well established [5]. Unlike the situation for the homogeneous case, in a bimaterial interface crack problem, the need for higher-order terms has not been felt until 1988. In 1988, Rice [6] gave the form of series solution that includes integer order terms. In 1993 Deng [7] reported another form of stress field equations in cartesian co-ordinates. Although the form of equations given by Deng is simpler than that stated by Rice, still it is not in a form that could be directly used for numerical computations. Ravichandran and Ramesh [8] have simplified the stress field equations of Deng suitable for experimental simplification, and the cartesian stress components of the stress field equation for the top half plane of an interface crack tangential to a bimaterial joint loaded at the boundary (see Figure 2.2), is given in the equation 2.1 as follows:

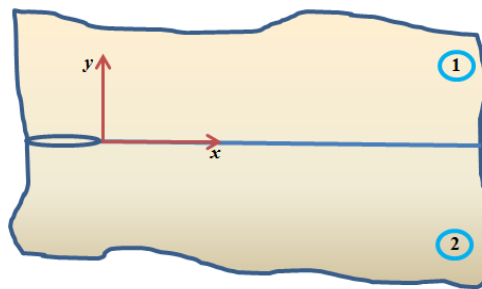


Figure 2.2: Co-ordinate system for interfacial crack

$$\begin{aligned}
\begin{pmatrix} (\sigma_{xx})_1 \\ (\sigma_{yy})_1 \\ (\tau_{xy})_1 \end{pmatrix} &= \sum_{n=0,2,4}^{\infty} \frac{K_{In}}{Q} r^{\frac{n-1}{2}} \left\{ \begin{aligned} &S \left\{ 3 \cos \left[ \left( \frac{n-1}{2} \right) \theta - \varepsilon \ln \frac{r}{L} \right] - (n-1) \sin \theta \sin \left[ \left( \frac{n-3}{2} \right) \theta - \varepsilon \ln \frac{r}{L} \right] + \right. \\ &S \left\{ \cos \left[ \left( \frac{n-1}{2} \right) \theta - \varepsilon \ln \frac{r}{L} \right] + (n-1) \sin \theta \sin \left[ \left( \frac{n-3}{2} \right) \theta - \varepsilon \ln \frac{r}{L} \right] - \right. \\ &S \left\{ -\sin \left[ \left( \frac{n-1}{2} \right) \theta - \varepsilon \ln \frac{r}{L} \right] - (n-1) \sin \theta \cos \left[ \left( \frac{n-3}{2} \right) \theta - \varepsilon \ln \frac{r}{L} \right] - \right. \\ &2\varepsilon \sin \theta \cos \left[ \left( \frac{n-3}{2} \right) \theta - \varepsilon \ln \frac{r}{L} \right] \left. \right\} - \frac{1}{S} \cos \left[ \left( \frac{n-1}{2} \right) \theta + \varepsilon \ln \frac{r}{L} \right] \\ &2\varepsilon \sin \theta \cos \left[ \left( \frac{n-3}{2} \right) \theta - \varepsilon \ln \frac{r}{L} \right] \left. \right\} + \frac{1}{S} \cos \left[ \left( \frac{n-1}{2} \right) \theta + \varepsilon \ln \frac{r}{L} \right] \\ &2\varepsilon \sin \theta \sin \left[ \left( \frac{n-3}{2} \right) \theta - \varepsilon \ln \frac{r}{L} \right] \left. \right\} + \frac{1}{S} \sin \left[ \left( \frac{n-1}{2} \right) \theta + \varepsilon \ln \frac{r}{L} \right] \end{aligned} \right. \\
&+ \sum_{n=1,3,5}^{\infty} \frac{K_{IIn}}{R} r^{\frac{n-1}{2}} \left\{ \begin{aligned} &4 \cos \left( \frac{n-1}{2} \right) \theta - (n-1) \sin \theta \sin \left( \frac{n-3}{2} \right) \theta \\ &(n-1) \sin \theta \sin \left( \frac{n-3}{2} \right) \theta \\ &-2 \sin \left( \frac{n-1}{2} \right) \theta - (n-1) \sin \theta \cos \left( \frac{n-3}{2} \right) \theta \end{aligned} \right. \\
&+ \sum_{n=0,2,4}^{\infty} \frac{K_{IIIn}}{Q} r^{\frac{n-1}{2}} \left\{ \begin{aligned} &S \left\{ 3 \sin \left[ \left( \frac{n-1}{2} \right) \theta - \varepsilon \ln \frac{r}{L} \right] + (n-1) \sin \theta \cos \left[ \left( \frac{n-3}{2} \right) \theta - \varepsilon \ln \frac{r}{L} \right] + \right. \\ &S \left\{ \sin \left[ \left( \frac{n-1}{2} \right) \theta - \varepsilon \ln \frac{r}{L} \right] - (n-1) \sin \theta \cos \left[ \left( \frac{n-3}{2} \right) \theta - \varepsilon \ln \frac{r}{L} \right] - \right. \\ &S \left\{ \cos \left[ \left( \frac{n-1}{2} \right) \theta - \varepsilon \ln \frac{r}{L} \right] - (n-1) \sin \theta \sin \left[ \left( \frac{n-3}{2} \right) \theta - \varepsilon \ln \frac{r}{L} \right] + \right. \\ &2\varepsilon \sin \theta \sin \left[ \left( \frac{n-3}{2} \right) \theta - \varepsilon \ln \frac{r}{L} \right] \left. \right\} + \frac{1}{S} \sin \left[ \left( \frac{n-1}{2} \right) \theta + \varepsilon \ln \frac{r}{L} \right] \\ &2\varepsilon \sin \theta \sin \left[ \left( \frac{n-3}{2} \right) \theta - \varepsilon \ln \frac{r}{L} \right] \left. \right\} - \frac{1}{S} \sin \left[ \left( \frac{n-1}{2} \right) \theta + \varepsilon \ln \frac{r}{L} \right] \\ &2\varepsilon \sin \theta \cos \left[ \left( \frac{n-3}{2} \right) \theta - \varepsilon \ln \frac{r}{L} \right] \left. \right\} + \frac{1}{S} \cos \left[ \left( \frac{n-1}{2} \right) \theta + \varepsilon \ln \frac{r}{L} \right] \end{aligned} \right. \\
&+ \sum_{n=1,3,5}^{\infty} \frac{K_{IIIn}}{R} r^{\frac{n-1}{2}} \left\{ \begin{aligned} &2 \sin \left( \frac{n-1}{2} \right) \theta + (n-1) \sin \theta \cos \left( \frac{n-3}{2} \right) \theta \\ &2 \sin \left( \frac{n-1}{2} \right) \theta - (n-1) \sin \theta \cos \left( \frac{n-3}{2} \right) \theta \\ &-(n-1) \sin \theta \sin \left( \frac{n-3}{2} \right) \theta \end{aligned} \right.
\end{aligned}$$

(2.1)



where,  $Q = 2\sqrt{2\pi} \cosh \pi\varepsilon$ ,  $R = \sqrt{2\pi} (1+w)$ ,  $S = e^{-\varepsilon(\pi-\theta)}$ ,  $\varepsilon = \frac{1}{2\pi} \ln \frac{(\mu_2\kappa_1 + \mu_1)}{(\mu_1\kappa_2 + \mu_2)}$ ,  $w = \frac{(1+\kappa_1)\mu_2}{(1+\kappa_2)\mu_1}$

$\kappa_i = \frac{3-\nu_i}{1+\nu_i}$  for plane stress and  $\kappa_i = 3-4\nu_i$  for plane strain. The SIF,  $K_{In}$  and  $K_{IIn}$  are the stress field parameters,  $\varepsilon$  is the bimaterial constant (oscillation index),  $L$  is the characteristic length,  $\mu_i$  is the shear moduli and  $\nu_i$  is the poisson's ratio of the two materials respectively ( $i = 1, 2$ ).

## 2.3 Experimental analysis

### 2.3.1 Specimen preparation

The simplest procedure for making a bimaterial joint is by joining two material halves with the help of an adhesive, provided that the adhesive is made from either of the parent material. If not, entire system will become a trimaterial. In the present study, epoxy is one of the parent material and it is also used as bonding medium. Figure 2.1 shows the specifications of bimaterial specimen under four point bending. Aluminum plate of required dimension is cut out from a big sheet and bonding surface is filed using 45 deg triangular file. Then epoxy specimen of same dimension is cut out from a casted sheet of epoxy and it's bonding surface is roughned by 220-grit emery. The roughned surfaces are cleaned with laboratory-grade isopropyl alcohol. Before bonding these two halves needs to be checked for the residual stress in epoxy in polariscope. If residual stress are present the model has to be heat treated in a furnace for 80 degrees for 2 hours. Then allow it to come to room temperature in the furnace itself. The model will be free of stress after this process and it is suitable for bonding.

The adhesive is then prepared by mixing epoxy resin (*C-51*) and hardener (*K-6*) in the weight ratio 10:1. The mixture is gently mixed by using glass rod for about 20 minutes. A thin Teflon tape (thickness 0.075 mm) equal to crack length of (3 mm and 19 mm) is placed on aluminium edge and silicone grease is applied on the teflone layer so that after curing, it can be easily removed from the interface. The adhesive prepared is then applied on the both the surfaces and bonded with a light pressure. The specimen is allowed to cure for 24 hours in a moisture free environment and after curing, teflon tape is removed, thereby forming the crack tip. The following figure 2.3 shows the bimaterial specimens made in house for the experimental analysis.

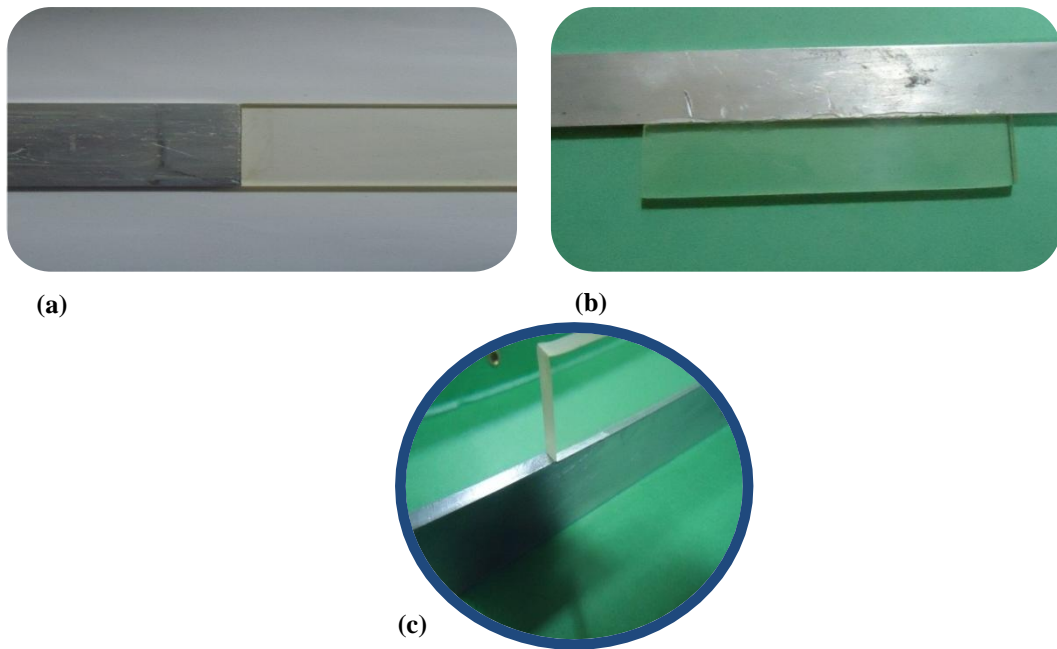


**Figure 2.3: Bimaterial specimens used for experimental analysis (a) Linear configuration (b) Stack configuration (c) Zoomed view of crack tip**

## **2.3.2 Total fringe order evaluation**

### **2.3.2.1 Ten-step method**

To evaluate SIF using digital photoelasticity, it is of great importance to obtain the total isochromatic fringe order information around the crack tip. Phase shifting techniques are one of the widely used methodologies for quantitative extraction of isochromatic and isoclinic parameter at every point (pixel) over the domain. The phase shifting algorithms basically provide isochromatic values in the form of wrapped phasemaps which are different from the conventional fringe patterns of photoelasticity. The wrapped phasemap essentially gives the fractional retardation at the point of interest. One of the main issues in isochromatic phasemap is how to interpret the sign of the fractional retardation calculated while unwrapping. Presently, use of quality guided approach for phase unwrapping that has been developed in other optical techniques has gained prominence in photoelasticity because of its autonomous capability.

In the present study, first, the total fringe order is obtained at each pixel over the entire model domain by employing ten-step phase shifting technique [18]. Recently, Ramji and Prasath [27] have recommended the use of ten-step phase shifting method for digital photoelastic applications involving manual polariscope. They have found that ten-step method enables to obtain both isoclinic and isochromatic parameter with

greater accuracy as compared to other phase shifting methods even in the presence of the various sources of error. Hence, in the present study ten-step method is used. The optical arrangements of the ten-step method are shown in Table 2.2. The first four steps correspond to the optical arrangements of the plane polariscope and the next six arrangements are based on a circular polariscope arrangement. For isoclinic parameter estimation,  $\theta_c$  is to be evaluated by atan2 () function. The isoclinic values thus obtained are then unwrapped and further used for isochromatic evaluation.

$$\theta_c = \frac{1}{4} \tan^{-1} \left( \frac{I_4 - I_2}{I_3 - I_1} \right) = \frac{1}{4} \tan^{-1} \left( \frac{\sin 4\theta \sin^2 \frac{\delta}{2}}{\cos 4\theta \sin^2 \frac{\delta}{2}} \right) \text{ for } \sin^2 \frac{\delta}{2} \neq 0 \quad (2.2)$$

$$\delta_c = \tan^{-1} \left( \frac{(I_9 - I_7) \sin 2\theta + (I_8 - I_{10}) \cos 2\theta}{I_5 - I_6} \right) \quad (2.3)$$

By using Eq. 2.2, isoclinic phase map is obtained and it has to be unwrapped by quality guided approach to remove the inconsistent zone. The unwrapped isoclinic values are then used to obtain isochromatic phase map without any ambiguous zones by using Eq. 2.3. Then the isochromatic phase map is unwrapped to get the whole field fringe order distribution. Adaptive quality guided algorithm is then used to unwrap both isoclinic data and isochromatic data at every pixel over the model domain. This continuous fringe order information is the most significant input for finding the SIF's.

Bimaterial specimen has been prepared as per the dimensions given in Figure 2.1 (a). Ten-step colour images in white light source are grabbed by the camera at a load of 125 N. Ten colour images as per Table 2.2 are shown in Appendix A. The system uses JAI 3CCD camera having the spatial resolution of 768×576 pixels. For data processing monochrome images are obtained from gray scale channel slot in the camera. Figure 2.4 shows the dark field colour image of bimaterial specimen and its zoomed image around the crack tip for the analysis purpose.

**Table 2.2: Optical arrangements of ten-step method**

$\alpha$	$\xi$	$\eta$	$\beta$	Intensity equation
$\pi/2$	-	-	0	$I_1 = I_b + I_a \sin^2 \frac{\delta}{2} \sin^2 2\theta$
$5\pi/8$	-	-	$\pi/8$	$I_2 = I_b + \frac{I_a}{2} \sin^2 \frac{\delta}{2} [1 - \sin 4\theta]$
$3\pi/4$	-	-	$\pi/4$	$I_3 = I_b + I_a \sin^2 \frac{\delta}{2} \cos^2 2\theta$
$7\pi/8$	-	-	$3\pi/8$	$I_4 = I_b + \frac{I_a}{2} \sin^2 \frac{\delta}{2} [1 + \sin 4\theta]$
$\pi/2$	$3\pi/4$	$\pi/4$	$\pi/2$	$I_5 = I_b + \frac{I_a}{2} (1 + \cos \delta)$
$\pi/2$	$3\pi/4$	$\pi/4$	0	$I_6 = I_b + \frac{I_a}{2} (1 - \cos \delta)$
$\pi/2$	$3\pi/4$	0	0	$I_7 = I_b + \frac{I_a}{2} (1 - \sin 2\theta \sin \delta)$
$\pi/2$	$3\pi/4$	$\pi/4$	$\pi/4$	$I_8 = I_b + \frac{I_a}{2} (1 + \cos 2\theta \sin \delta)$
$\pi/2$	$\pi/4$	0	0	$I_9 = I_b + \frac{I_a}{2} (1 + \sin 2\theta \sin \delta)$
$\pi/2$	$\pi/4$	$3\pi/4$	$\pi/4$	$I_{10} = I_b + \frac{I_a}{2} (1 - \cos 2\theta \sin \delta)$

$\alpha$  - polarizer angle.  
 $\xi$  - input quarter wave plate angle.  
 $\eta$  - output quarter wave plate angle.  
 $\beta$  - analyzer angle.

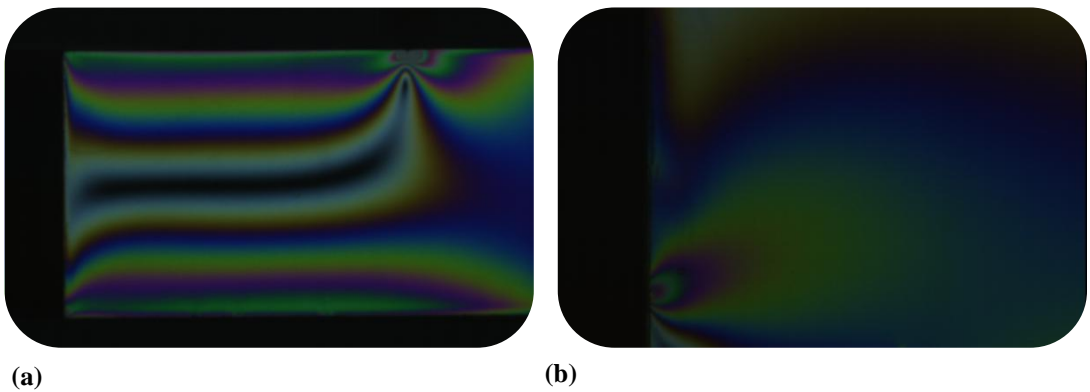


**Figure 2.4: Dark field colour image of bimaterial specimen at 125 N (a) Full isochromatic view subjected to four point bending (b) Zoomed part near the crack tip**

### **2.3.2.2 Three fringe photoelasticity**

Use of a colour code to identify fringe direction and assigning the total fringe order has become an accepted method in conventional photoelasticity. TFP is an extension of this technique in digital domain. The total fringe order at a point of interest in the actual model is then established by comparing the RGB values at the point of interest with that of the calibration table. The colours tend to merge beyond fringe order three, and hence the technique is termed as TFP. TFP can give total fringe order from a single isochromatic dark field image. This technique is very useful in dealing with transient problems, as the process is instantaneous.

In TFP one has to compare the RGB values of a point with the calibrated RGB values assigned with known fringe orders so as to determine fringe order at the given point. Use of single calibration table can help to simplify the use of TFP in an industrial environment. A simple way to use a single table is to modify the RGB variation of calibration specimen recorded equivalent to that as if the application specimen material has been used for making the calibration specimen. This can be done if the shift in individual RGB values due to tint variation between the calibration and application specimen is estimated and incorporated suitably.

While assigning fringe orders in TFP, discontinuities in fringe orders are obtained, which leads to streaks in the total fringe order plot. To maintain the continuous variation of fringe order researchers have used the help of neighbourhood fringe order with an additional term, which can remove the discontinuities in the fringe order in TFP. This methodology is termed as RTFP [15].

Bimaterial specimen has been made as per the dimensions given in Figure 2.1 (b). Dark field colour image in white light source was taken by the camera at a load of 250 N. The system uses JAI 3CCD camera having the spatial resolution of 768×576 pixels. Figure 2.5 shows the dark field colour image of bimaterial specimen and its zoomed image around the crack tip for the analysis purpose.

### **2.3.3 Photoelastic determination of SIF**

As discussed earlier the whole field isochromatic data is obtained using the ten-step method for linear configuration and by RTFP for stack configuration. An over-deterministic least squares approach is used to evaluate the multi-parameters governing the stress field iteratively. Although data can be collected anywhere from the fringe field, for easy convergence, it has been reported that the fringe order and the

corresponding positional coordinates need to be collected such that, when plotted they capture the basic geometric features of the fringe field. As data needs to be collected nearer to crack tip for each load step, manual data collection along the thinned fringe skeletons would not only be erroneous but also it is tedious. Hence, automated data collection is implemented. The automated data collection software developed in house using VC++ has an interactive module to remove outliers.

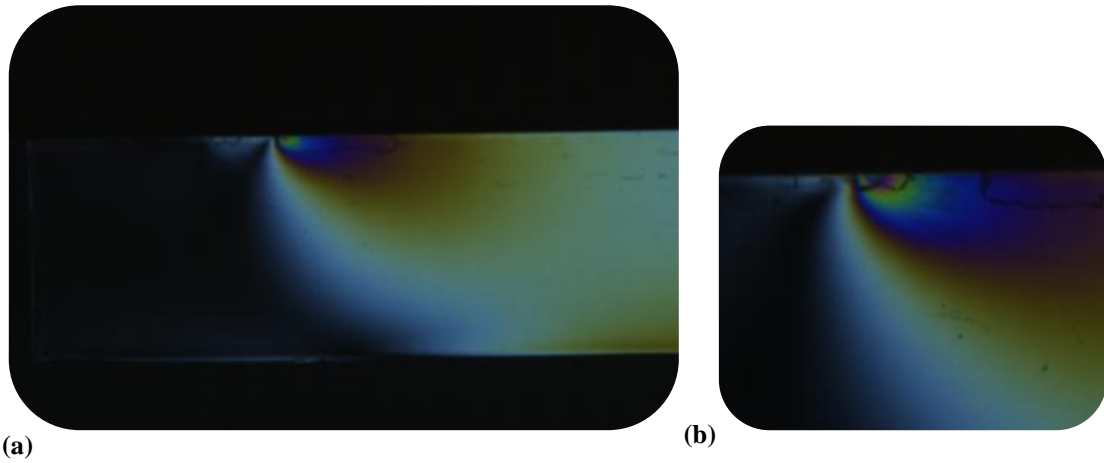


**Figure 2.5: Dark field color image of bimaterial specimen at 250 N (a) Full isochromatic view subjected to four point bending (b) Zoomed part near the crack tip**

The fringe orders and coordinates defining the positions of various data points surrounding crack tip are selected automatically in the range  $0.05 < r/a < 0.7$  and they are utilized for SIF evaluation using the method of least squares technique. Since the number of parameters required for modelling the stress field is not known a priori, the iteration is started with two parameters stress field equations. The iteration is stopped using the fringe order error minimization criteria [28]. Using the solution of the parameters thus obtained as starting values, the number of parameters in each series is iteratively increased until the convergence error obtained is of the order of 0.05 or less [28].

#### **2.4 Numerical evaluation of SIF**

In the present work we have used VCCI technique to estimate the SIF's of an interface crack. This method is purely based on energy release rate approach. This would compute the mixed mode SIF's from mixed mode energy release rates of interfacial crack, which are easily obtained from the crack opening displacements and

the nodal forces at and ahead of the crack tip, in the FE model. SIF obtained by above method has been compared using  $J$ -integral approach as well.

### 2.4.1 VCCI technique

According to Irwin, the work required to extend a crack by an infinitesimal distance  $\Delta$  is equal to the work required to close the crack to its original length. Thus energy release rate (ERR) for mode I and mode II deformations can be expressed as,

$$G_I = \frac{1}{2\Delta} \int_0^{\Delta} \sigma_{22}(r) \delta_2(\Delta - r) dr$$

$$G_{II} = \frac{1}{2\Delta} \int_0^{\Delta} \sigma_{12}(r) \delta_1(\Delta - r) dr$$

$$G_{I-II} = \frac{1}{2\Delta} \int_0^{\Delta} [\sigma_{12}(r) \delta_2(\Delta - r) + \sigma_{22}(r) \delta_1(\Delta - r)] dr$$
(2.4)

The procedure to obtain these energy release rates from FE solutions were given by Rybicki and Kanninen and Raju. They have calculated the energy release rates for mode I problem from nodal forces at and ahead of the crack tip and displacements near the crack tip (along the crack axis). Referring to the Figure 2.6, ERR's are given as,

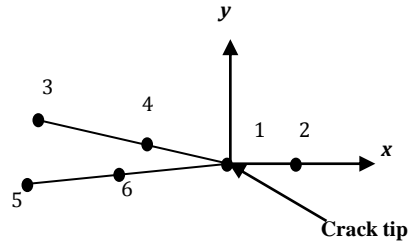


Figure 2.6: Coordinate system for bimaterial crack

$$G_I = \frac{1}{2\Delta} [f_{y1}(v_5 - v_3) + f_{y2}(v_6 - v_4)]$$

$$G_{II} = \frac{1}{2\Delta} [f_{x1}(u_5 - u_3) + f_{x2}(u_6 - u_4)]$$

$$G_{I-II} = \frac{1}{2\Delta} [f_{x1}(v_5 - v_3) + f_{x2}(v_6 - v_4) + f_{y1}(u_5 - u_3) + f_{y2}(u_6 - u_4)]$$
(2.5)

where  $f_x, f_y$  are force components and  $u, v$  are displacements along  $x$  and  $y$  directions respectively. The subscripts 1,2...6 represents respective node numbers in FE model. Basic singular stress field equations obtained by Rice and Sih, can be written as (at  $\theta = 0$ ),

$$\sigma_{22} + i\sigma_{12} = \frac{K}{\sqrt{2\pi r}} r^{i\varepsilon} \quad K = K_1 + iK_2 \quad (2.6)$$

where  $K$  is the complex SIF. The crack opening displacements at a distance  $r$  behind the crack tip is given by,

$$\delta_2 + i\delta_1 = \frac{c_1 + c_2}{2\sqrt{2\pi}(1 + 2i\varepsilon) \cosh(\pi\varepsilon)} K \sqrt{r} r^{i\varepsilon} \quad (2.7)$$

where the compliance parameters,  $c_i$ 's are

$$c_1 = \frac{\kappa_1 + 1}{\mu_1} \quad c_2 = \frac{\kappa_2 + 1}{\mu_2} \quad (2.8)$$

The  $K_I$  and  $K_{II}$  parameters are obtained form ERR as per the procedure given by Chow and Atluri [26]. They have developed a linear relationship between energy release rates and SIF's which is clearly explained in Appendix B. SIF's are obtained by solving these equations.

#### 2.4.2 Finite element modeling of bimaterial

In the present work modeling has been done in ANSYS version 13 software. For meshing eight noded quadratic element (plane-183) is used. Areas near to the crack tip is meshed by elements having size 0.2 mm and maintaining an aspect ratio of one, and areas far away from crack tip is meshed by relatively course mesh with appropriate spacing ratio. Areas having dissimilar meshes are joined together by multipoint constraint (MPC) algorithm. After applying boundary conditions, model is checked for displacement continuity across the dissimilar mesh interface. Total number of elements for this FE model is 10382 for linear configuration and 13408 for stack configuration. Figure 2.7 (a) shows the FE mesh for the bimaterial and Figure 2.7 (b) shows zoomed mesh near the crack tip for linear configuration. Similarly Figure 2.8 shows the FE mesh for stack configuration.



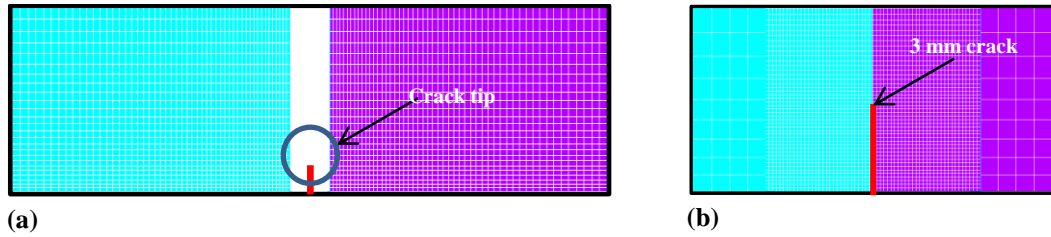


Figure 2.7: FE model of bimaterial specimen (linear configuration) (a) Complete meshed model (b) Zoomed part near crack tip

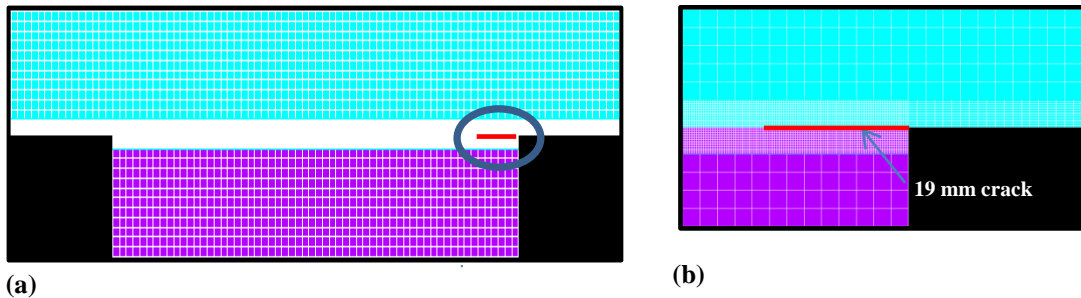


Figure 2.8: FE model of bimaterial specimen (stack configuration) (a) Complete meshed model (b) Zoomed part near crack tip

In the present work modeling has also be done in ABAQUS and SIF is evaluated by  $J$ -integral method. For meshing four noded linear element (CPS4R) has been used. Rectangular mapped mesh is preferred and element size is maintained to be 1 mm. Total number of elements for this FE model is 12600 for linear configuration and 10000 for stack configuration. Figure 2.9 (a) shows the FE mesh for the bimaterial and Figure 2.9 (b) shows zoomed mesh near the crack tip for linear configuration. Similarly Figure 2.10 shows the FE mesh for stack configuration.

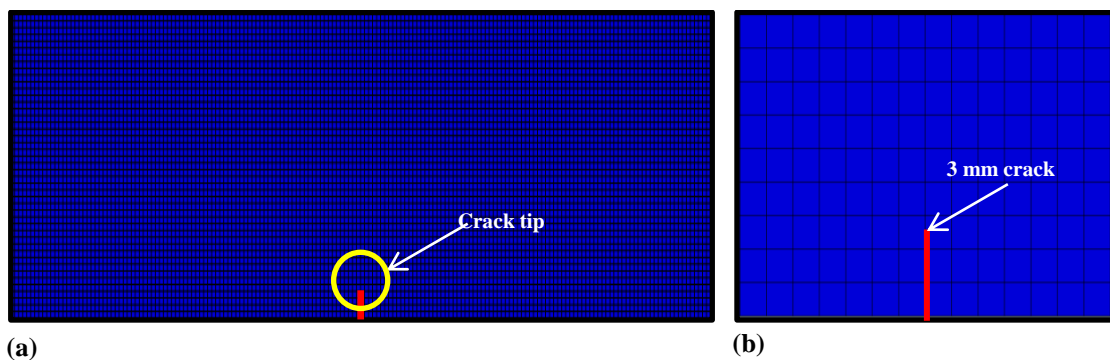
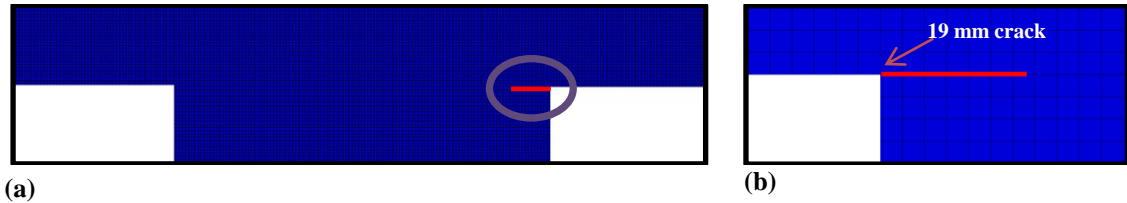


Figure 2.9: FE model of bimaterial specimen (linear configuration) (a) Complete meshed model (b) Zoomed part near crack tip



**Figure 2.10: FE model of bimaterial specimen (stack configuration) (a) Complete meshed model (b) Zoomed part near crack tip**

## 2.5 Results and discussions

### 2.5.1 Experimental results

#### 2.5.1.1 Linear configuration

As discussed earlier the whole field isochromatic data is obtained using the ten-step method. Figure 2.11 shows the unwrapped isochromatic and isoclinic phase map and also includes the MATLAB plot for the four point bend specimen. Figure 2.11 (a) shows the wrapped isoclinic phasemap and the unwrapped isoclinic phasemap is shown in Figure 2.11 (b). The unwrapped isoclinic is used to get the isochromatic phasemap without any ambiguity and it is shown in Figure 2.11 (c). This needs to be unwrapped to get the total fringe order over the model domain and it is shown in Figure 2.11 (d) as gray scale plot and the MATLAB plot is shown in Figure 2.11 (e). The unwrapping of isoclinic isochromatic data is done using the adaptive quality guided phase unwrapping algorithm. Figure 2.12 shows the comparison between the bright, dark field reconstructed image using the experimentally obtained parameters with the collected data points echoed back. The convergence is obtained at the four parameter.

#### 2.5.1.2 Stack configuration

As discussed earlier the whole field isochromatic data is obtained using the RTFP method. The Figure 2.13 shows the total fringe order plot obtained from RTFP. Automatic data collection is carried out for fringes 0.5, 1.0 and 1.5. Using collected data points SIF is evaluated by employing least squares technique. Figure 2.14 shows the comparison between the dark, bright field reconstructed image using the experimentally obtained parameters with the collected data points echoed back. The convergence is obtained at the six parameter.

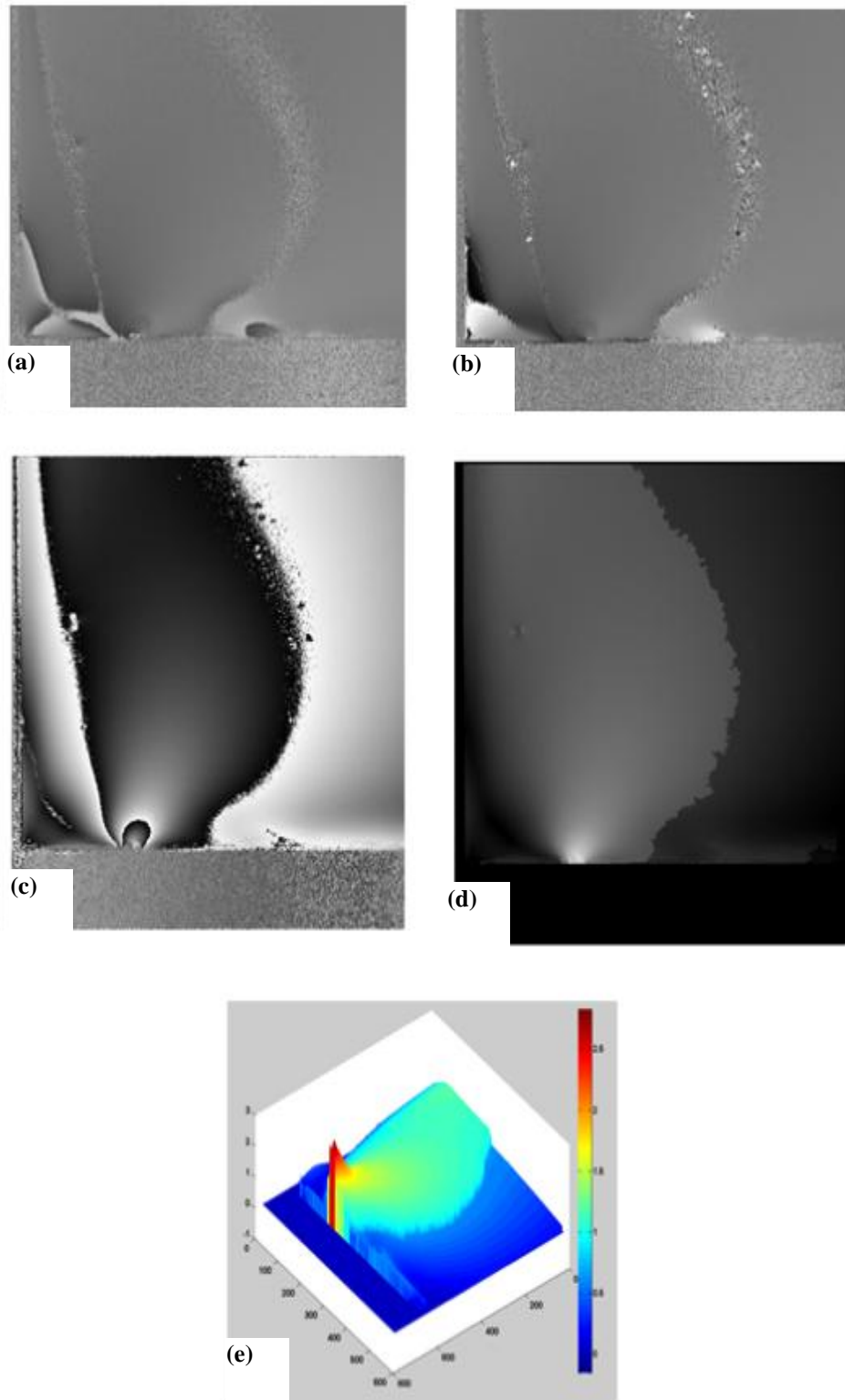


**Figure 2.11: Experimental data from photoelasticity using ten-step method (a) Wrapped isoclinic phase map (b) Unwrapped isoclinic phase map (c) Isochromatic phase map (d) Grey scale plot for unwrapped isochromatic phase map (e) MATLAB plot**

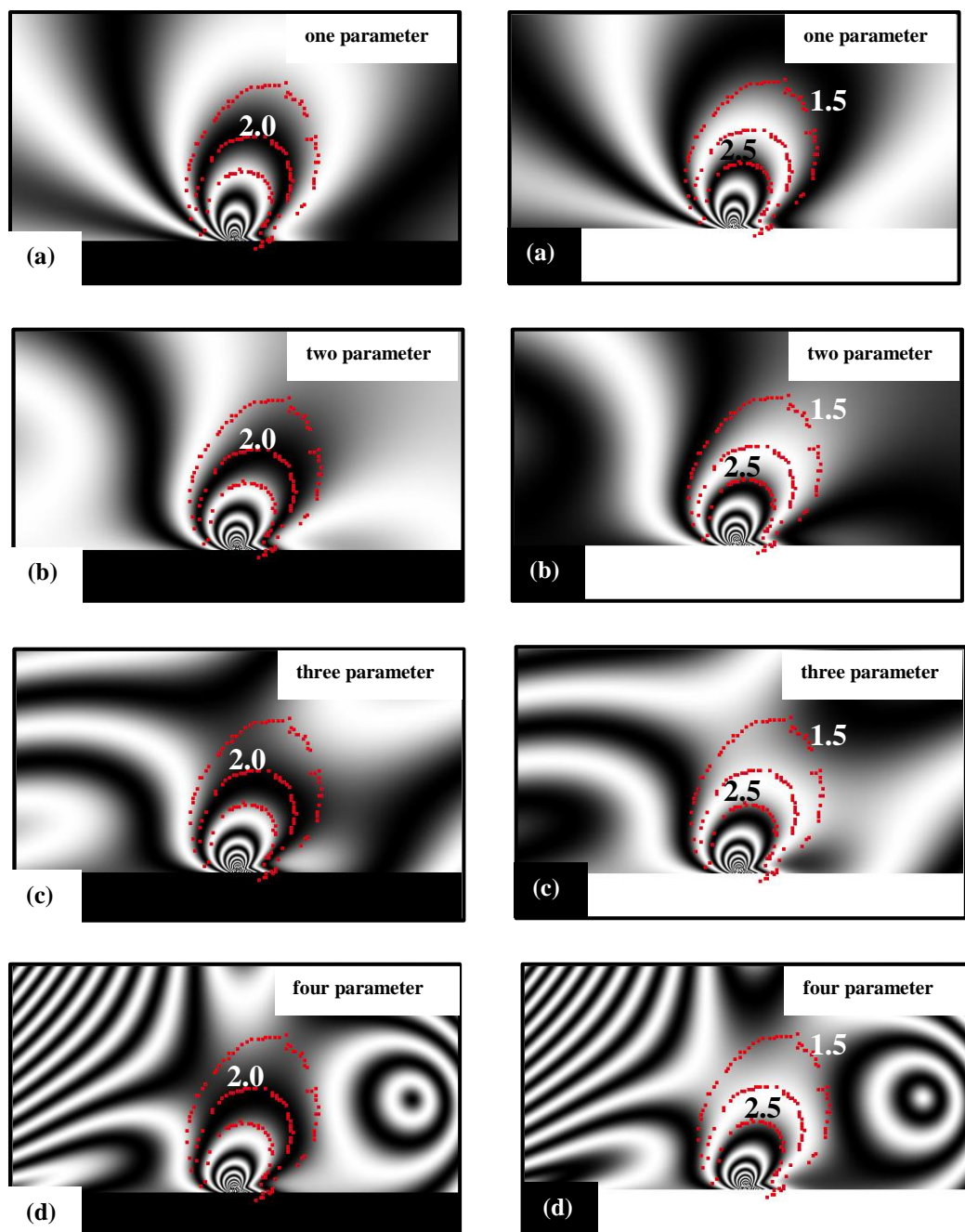


Figure 2.12: Theoretically reconstructed isochromatic fringe patterns (dark field and bright field) with data points superimposed for (a) One parameter (b) Two parameter (c) Three parameter (d) Four parameter

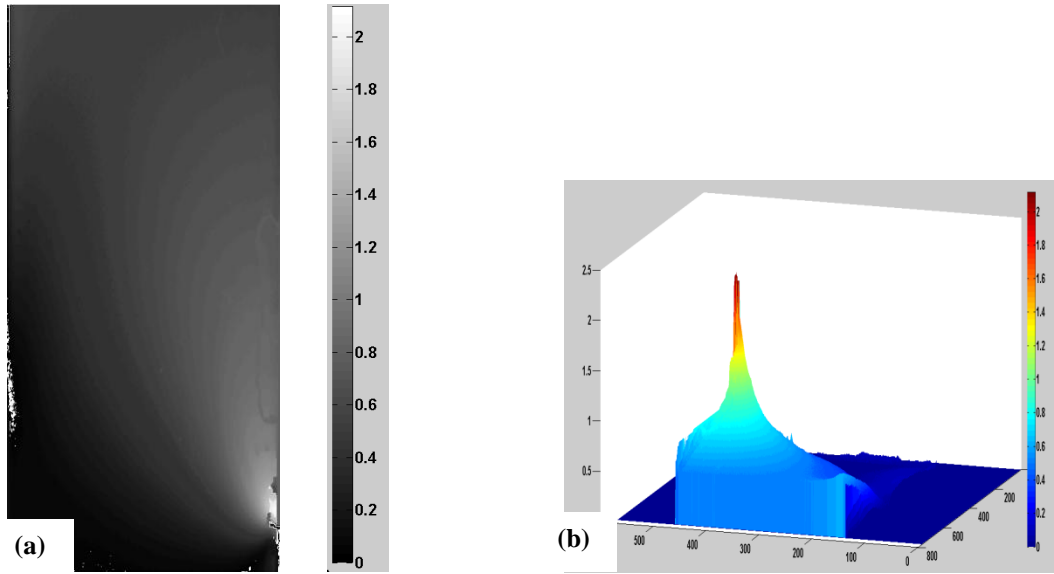


Figure 2.13: Total fringe order plot for stack configuration using TFP (a) Gray scale plot (b) 3D plot of total fringe order

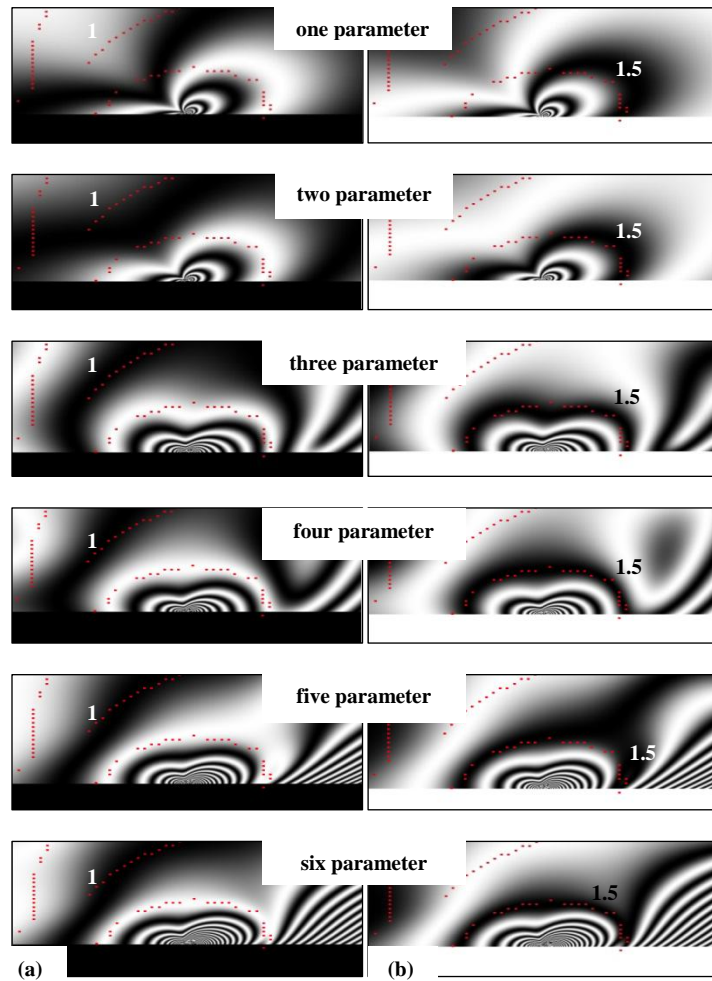


Figure 2.14: Theoretically reconstructed isochromatic fringe patterns (dark and bright field) with data points superimposed for six parameter (a) Dark field (b) Bright field

### 2.5.2 Comparison of experimental and numerical results

Table 2.3 shows the SIF evaluated by different approaches. Looking at the table SIF from VCCI and  $J$ -integral approach compare very well but with digital photoelasticity value they slightly differ. In all the three cases  $K_I$  is higher than  $K_{II}$  for both the configuration denoting the dominance of mode I.

**Table 2.3: Comparison of SIF**

<b>SIF (MPa<math>\sqrt{m}</math>)</b>	<b>Digital photoelasticity</b>	<b>VCCI technique</b>	<b><math>J</math>-integral method</b>
<b>Linear configuration</b>	$K_I = 0.256$ $K_{II} = 0.037$	$K_I = 0.3011$ $K_{II} = 0.0278$	$K_I = 0.3122$ $K_{II} = 0.0269$
<b>Stack configuration</b>	$K_I = 0.258$ $K_{II} = 0.137$	$K_I = 0.377$ $K_{II} = 0.1579$	$K_I = 0.369$ $K_{II} = 0.1569$

### 2.6 Closure

Bimaterial models made of Al / Epoxy are analysed. Experimentally SIF's has been evaluated using over-deterministic approach involving multi-parameter stress field equations of Deng. Total fringe order for linear configuration is estimated by ten-step phase shifting technique while for stack configuration RTFP is used. Fourth parameter seems to be accurate in capturing the fringe field for linear configuration and sixth parameter for stack configuration. Numerically SIF's were also evaluated using VCCI method and  $J$ -integral approach. It is found that there is no appreciable variation between VCCI and  $J$ -integral approach. But appreciable difference exists between the values obtained from digital photoelasticity and numerical values but it is of the same order. Percentage error in  $K_I$  and  $K_{II}$  are 15% and 25% respectively for linear configuration and 30% and 13% respectively for stack configuration. An improved FE model needs to be developed by incorporating an interfacial layer.

# Chapter 3

## Experimental and Numerical Evaluation of Order of Singularity in a Bimaterial Interface Corner

### 3.1 Introduction

To know about interfacial fracture mechanics has become important as there exist wide applications in the field of electronic packaging. As mentioned in the previous chapter a single electronic chip has been made with different interconnects which forms different interfaces of dissimilar materials. Also adhesive bonding of dissimilar materials have been used in numerous aircrafts primary structures. Shear failure is commonly observed at the bonding interface on metal / polymer joints. Due to the complex geometry as well as different mechanical properties along the interface, getting knowledge of fracture parameters is important and equally difficult. Studies have found that bimaterial corners (wedges) will give rise to stress concentrations and are almost similar to a crack. But in the case of corner it will have an order of singularity between 0 and 1. The order of singularity purely depends on material properties and geometry. It is totally independent of loading condition and type of load. It is well known that stress fields at the interface corners exhibits a singular behaviour for a linear elastic material that is proportional to  $r^\lambda$ , where  $r$  represents the distance from the interface corner. The failure due to stress concentration usually originates at singular stress point, and the knowledge of interfacial fracture mechanics is important to understand the failure mechanisms in corners of interface.

Analytical studies for finding the order of singularity for a homogeneous material wedge has been done in 1996 [23]. In 2005, Yaping Luo and Ganesh Subbarayan [24] has extended this work for dissimilar materials and they estimated corner SIF for a dissimilar material wedges involving FEA. In the present work the procedure for finding  $\lambda$  value for Aluminum / Epoxy bimaterial models is done by same approach and stress field (maximum shear stress) has been plotted around the bimaterial corner by both experimental and numerical method. Digital photoelasticity is used for finding the maximum shear stress distribution around the corner of bimaterial and it has been validated by FEM. As discussed in chapter 1, TSV technique mainly uses linear

configuration and stack configuration for manufacturing the interconnects. So in the present study linear as well as stack configuration is carried out. The dimensions of these bimaterial configurations are given in the Figure 3.1 and they do not contain any crack. Analysis is carried out at 150 N for linear configuration while at 300 N for stack configuration under four point bending. In the present work, we used linear elastic fracture mechanics frame work and plain strain condition is assumed.

In the present chapter, deals with analytical determination of singularity value, experimental analysis by digital photoelasticity (total fringe order evaluation by RTFP), numerical analysis by FEM. Prediction of scale factor for bimaterial using digital photoelasticity and FEM is explained and finally corner stress intensity is evaluated.

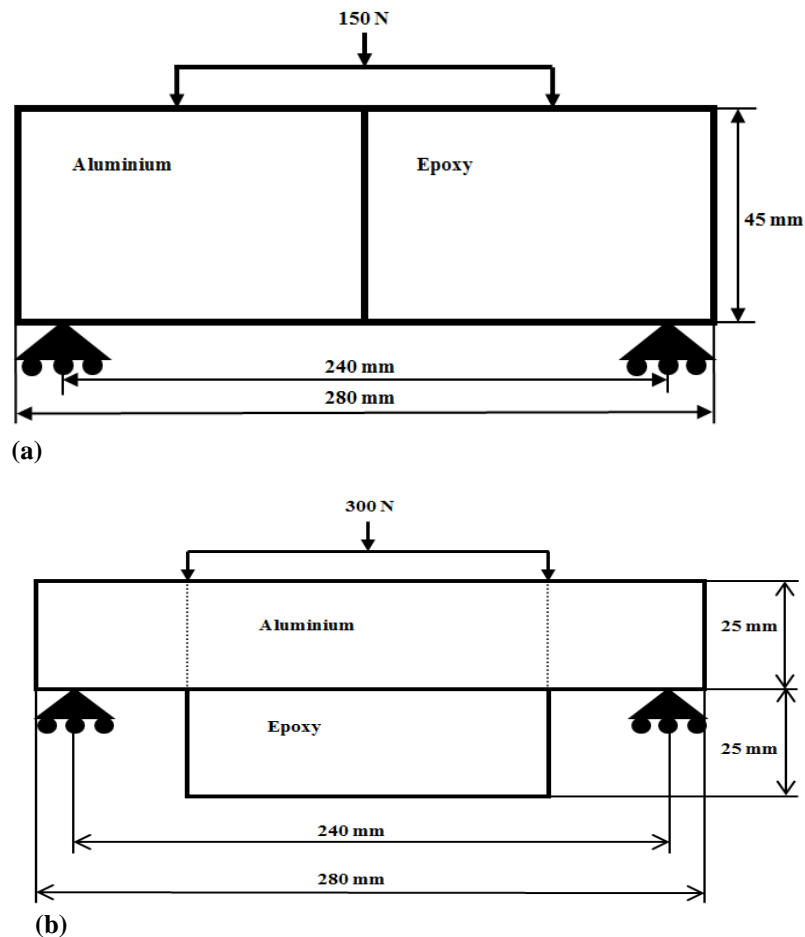


**Figure 3.1: Bimaterial configurations used for study (a) Linear configuration (b) Stack configuration**



### 3.2 Stress field equations for an interfacial corner

Consider a multi-material wedge in polar coordinate system  $(r, \theta)$  as shown in the Figure 3.2.

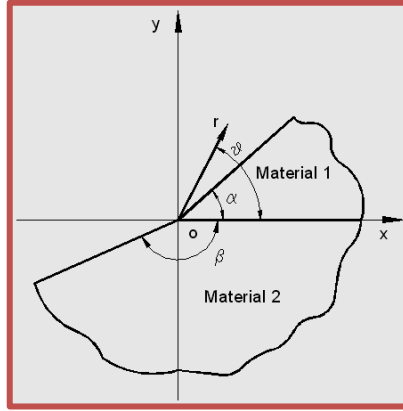


Figure 3.2: Coordinate system for bimaterial wedge problem

Let  $i$  denote the different materials present in the wedge. The stress fields and displacement fields for a corner of dissimilar materials is developed by extending the work of Seweryn and Molski by Yaping and Ganesh as given below:

$$\begin{aligned}
 u_i &= r_i^\lambda \left[ A_i \cos(1+\lambda)\theta_i + B_i \sin(1+\lambda)\theta_i + C_i \cos(1-\lambda)\theta_i + D_i \sin(1-\lambda)\theta_i \right], \\
 u_{\theta_i} &= r_i^\lambda \left[ B_i \cos(1+\lambda)\theta_i - A_i \sin(1+\lambda)\theta_i + \nu_{2_i} D_i \cos(1-\lambda)\theta_i - \nu_{2_i} C_i \sin(1-\lambda)\theta_i \right], \\
 \sigma_{r_i} &= r_i^{\lambda-1} \mu_i \left[ 2\lambda A_i \cos(1+\lambda)\theta_i + 2\lambda B_i \sin(1+\lambda)\theta_i - (3-\lambda)(1-\nu_{2_i}) C_i \cos(1-\lambda)\theta_i \right. \\
 &\quad \left. - (3-\lambda)(1-\nu_{2_i}) D_i \sin(1-\lambda)\theta_i \right], \\
 \sigma_{\theta_i} &= r_i^{\lambda-1} \mu_i \left[ -2\lambda A_i \cos(1+\lambda)\theta_i - 2\lambda B_i \sin(1+\lambda)\theta_i - (1+\lambda)(1-\nu_{2_i}) C_i \cos(1-\lambda)\theta_i \right. \\
 &\quad \left. - (1+\lambda)(1-\nu_{2_i}) D_i \sin(1-\lambda)\theta_i \right] \\
 \tau_{r\theta_i} &= r_i^{\lambda-1} \mu_i \left[ -2\lambda A_i \sin(1+\lambda)\theta_i + 2\lambda B_i \cos(1+\lambda)\theta_i - (1-\lambda)(1-\nu_{2_i}) C_i \sin(1-\lambda)\theta_i \right. \\
 &\quad \left. + (1-\lambda)(1-\nu_{2_i}) D_i \cos(1-\lambda)\theta_i \right]
 \end{aligned} \tag{3.1}$$

where  $A, B, C, D$  denotes unknown parameters in the bimaterial system and it depends on the loading conditions and order of singularity, which intern depends on the scale parameter suppose  $k$ , which has to be evaluated experimentally or numerically.

### 3.3 Analytical determination of order of singularity

In general singularity is a measure denoting the severity of stress field around a zone having high stress gradient. In the case of crack in a homogeneous medium order of singularity is 0.5, while for a bimaterial case singularity will be a number between 0 and 1. In the case of bimaterial wedge with only one bonded interface (as shown in Fig.3.2),

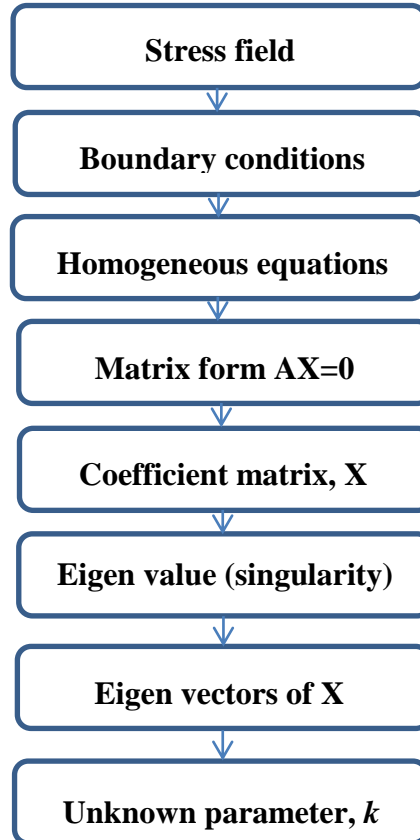
one can apply two sets of boundary condition. The first set is continuity condition at the material interface and the second set is traction free condition at the two free surfaces, as shown below.

$$u_{r_1} = u_{r_2}, u_{\theta_1} = u_{\theta_2}, \sigma_{\theta_1} = \sigma_{\theta_2}, \tau_{r\theta_1} = \tau_{r\theta_2} \text{ at } \theta = 0 \quad (3.2a)$$

$$\begin{aligned} \sigma_{\theta_1} &= 0, \tau_{r\theta_1} = 0 \text{ at } \theta = \alpha; \\ \sigma_{\theta_2} &= 0, \tau_{r\theta_2} = 0 \text{ at } \theta = -\beta; \end{aligned} \quad (3.2b)$$

One can impose above mentioned boundary conditions on displacement as well as stress field equations, and it will yield eight homogeneous equations. For nontrivial solution of constants,  $A, B, C, D$ , the determinant of eigen value problem should vanish, which results in a nonlinear equation for  $\lambda$ . Solving for this equation one can find the singularity value(s). Using obtained eigen value(s) one can obtain the corresponding eigen vectors ( $A, B, C, D$ ) in terms of a scale parameter  $k$ .

The value of  $k$  will depend upon loading conditions, material properties and geometry of bimaterial corner. It can be found out from experiments or FEM by obtained value of singularity. The following flow chart shows the deduction procedure for singularity and  $k$  values for a general bimaterial problem.



Flow chart showing determination of singularity

### 3.4 Experimental analysis

#### 3.4.1 Specimen preparation

The simplest procedure for making a bimaterial joint is by joining two material halves with the help of an adhesive, provided that the adhesive is made from either of the parent material. If not, entire system will become a trimaterial. In the present study, epoxy is one of the parent material and the same is used as bonding medium. Figure 3.1 shows the specifications of bimaterial specimen subjected to four point bending. The same procedure is followed as explained in the previous chapter with an exception of not introducing any crack at the interface. Figure 3.3 shows the bimaterial specimens being made for the study.

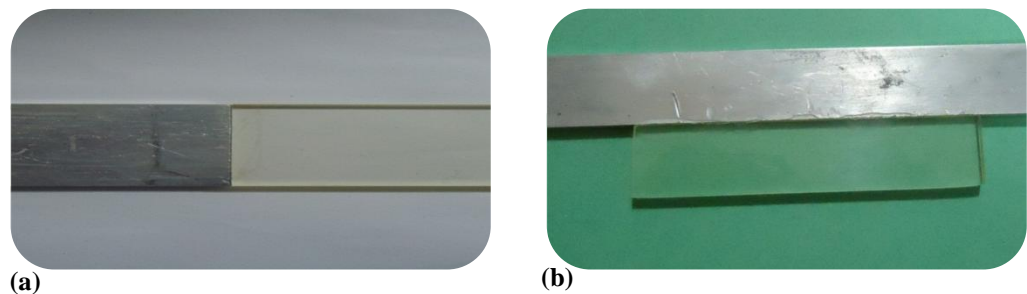
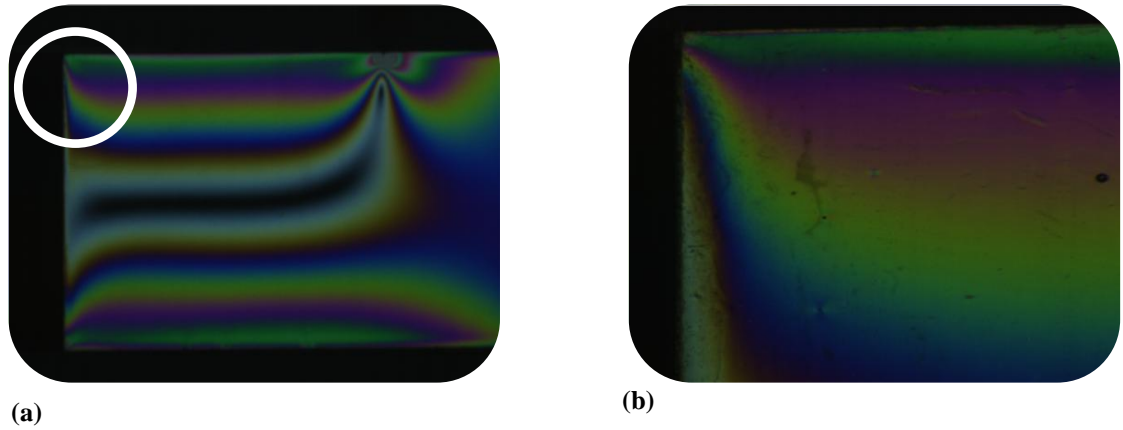


Figure 3.3: Bimaterial specimens used for experimental analysis (a) Linear configuration (b) Stack configuration

#### 3.4.2 Total fringe order estimation

For extraction of data around the bimaterial corner, it is of great importance to obtain the total isochromatic fringe order information around that corner. Phase shifting techniques are one of the widely used methodologies for quantitative extraction of isochromatic and isoclinic parameter at every point (pixel) over the domain. The phase shifting algorithms basically provide isochromatic values in the form of wrapped phasemaps which are different from the conventional fringe patterns of photoelasticity. But one disadvantage with phase shifting technique is that it requires more number of images to be grabbed for analysis purpose. By the invention of colour image processing techniques use of colour image to extract the data has gained importance and one can get total fringe order over entire model domain by grabbing single image. Three fringe photoelasticity is one among them which can be applied confidently for problems having less than three fringe orders. So in the present study RTFP is used for total fringe order estimation for both the configuration. Bimaterial specimens have been prepared as per the dimensions given in Figure. 3.1. Dark field colour image in white light source is

taken by the camera at a load of 150 N for linear configuration and 300 N for stack configuration. The system uses JAI 3CCD camera having the spatial resolution of 768×576 pixels. Figure 3.4 and figure 3.5 shows the dark field colour image of bimaterial specimens and its zoomed image around the corner for the analysis purpose.



**Figure 3.4:** Dark field image taken at 150 N for linear configuration (a) Full dark field (b) Zoomed part near the corner

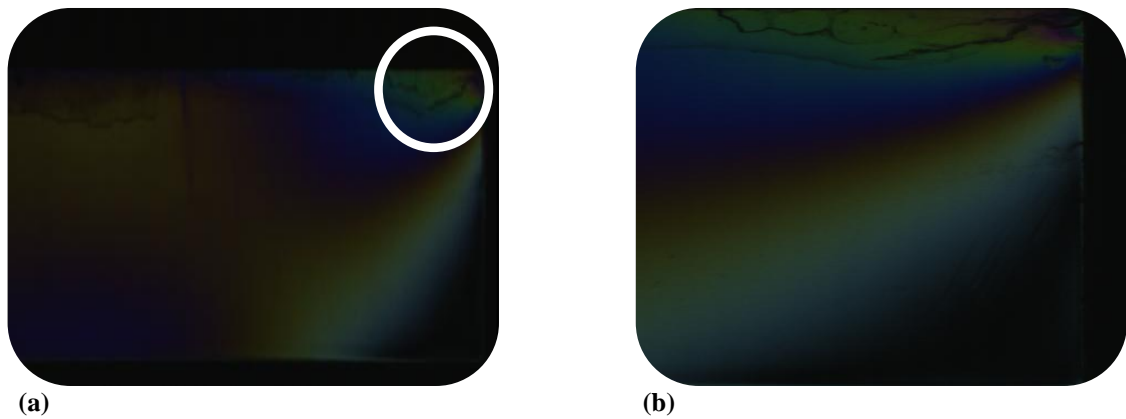


**Figure 3.5:** Dark field image taken at 300 N for stack configuration (a) Full dark field (b) Zoomed part near the corner

### 3.5 Finite element modeling of bimaterial

In the present work modeling has been done in ANSYS version 13 software. For meshing eight noded quadratic element (plane 183) is used. Area near to the interface is meshed by elements having size 0.2 mm having an aspect ratio of one, and zones far away from crack tip is meshed by relatively course mesh with proper spacing ratio. Areas having dissimilar meshes are joined together by multipoint constraint (MPC) algorithm. After applying boundary conditions, model is checked for displacement continuity across the dissimilar mesh interface. Total number of elements for this FE

model is 10382 for linear configuration and 13408 for stack configuration. Figure 3.6(a) shows the FE mesh for the bimaterial and Figure 3.6(b) shows zoomed mesh near the corner for linear configuration. Similarly figure 3.7 shows the FE mesh for stack configuration.

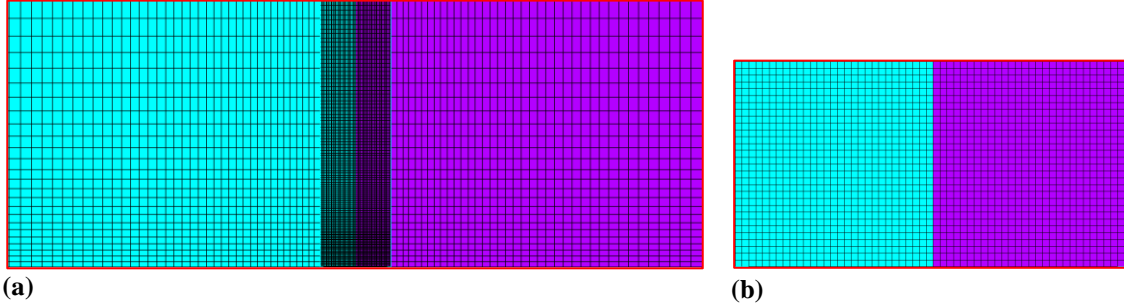


Figure 3.6: FE model of bimaterial specimen having linear configuration (a) Full meshed model  
(b) Zoomed part near corner

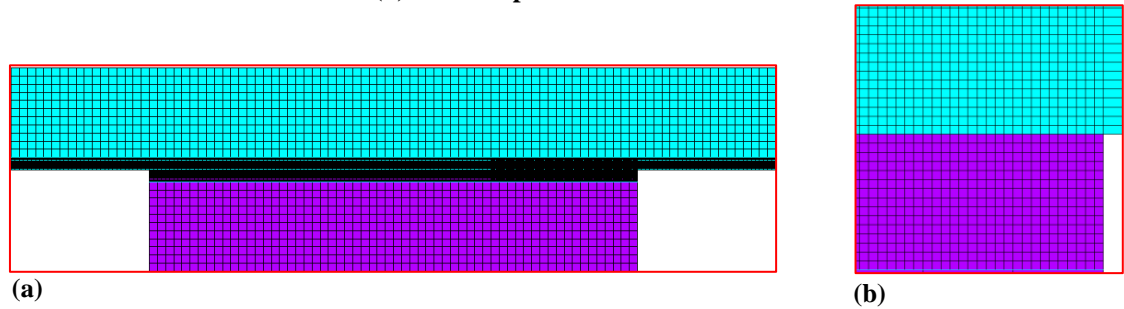


Figure 3.7: FE model of bimaterial specimen having stack configuration (a) Full meshed model  
(b) Zoomed part near corner

## 3.6 Results and discussions

### 3.6.1 Analytical determination of singularity

Consider the co-ordinate system for linear configuration as shown in Figure 3.8(a). In the case of bimaterial wedge with only one bonded interface (see Fig.3.2), one can apply two sets of boundary condition. The first set is continuity condition at the material interface and the second set is traction free condition at the two free surfaces as given in Eq.3.3.

$$u_{r_1} = u_{r_2}, u_{\theta_1} = u_{\theta_2}, \sigma_{\theta_1} = \sigma_{\theta_2}, \tau_{r\theta_1} = \tau_{r\theta_2} \text{ at } \theta = 0 \quad (3.3a)$$

$$\sigma_{\theta_1} = 0, \tau_{r\theta_1} = 0 \text{ at } \theta = \frac{\pi}{2}; \quad (3.3b)$$

$$\sigma_{\theta_2} = 0, \tau_{r\theta_2} = 0 \text{ at } \theta = -\frac{\pi}{2};$$

After implementing the procedure given in the flow chart, one can get the singularity value(s). Figure 3.8 (b) shows the eigen value (singularity) determination for linear configuration, the value at which determinant of matrix A should be zero.

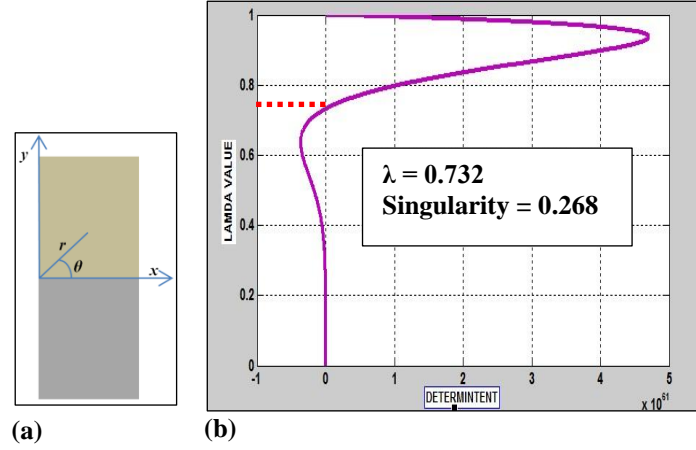


**Figure 3.8: Eigen value determination for linear configuration (a) Co-ordinate system for linear configuration (b) Graph showing obtained value of singularity**

Consider the coordinate system for stack configuration as shown in Figure 3.9 (a). In the case of bimaterial wedge with only one bonded interface (as shown in Fig.3.2), one can apply two sets of boundary condition. The first set is continuity condition at the material interface and the second set is traction free condition at the two free surfaces given below in Eq. 3.4.

$$u_{r_1} = u_{r_2}, u_{\theta_1} = u_{\theta_2}, \sigma_{\theta_1} = \sigma_{\theta_2}, \tau_{r\theta_1} = \tau_{r\theta_2} \text{ at } \theta = 0 \quad (3.4a)$$

$$\begin{aligned} \sigma_{\theta_1} = 0, \tau_{r\theta_1} = 0 \text{ at } \theta = \frac{\pi}{2}; \\ \sigma_{\theta_2} = 0, \tau_{r\theta_2} = 0 \text{ at } \theta = -\pi; \end{aligned} \quad (3.4b)$$

After implementing the procedure shown in the flow chart, one can get the singularity value(s). Figure 3.9 (b) shows the eigen value (singularity) determination for stack configuration, the value at which determinant of matrix A should be zero. The obtained value of singularity for linear configuration is 0.268 and for stack configuration it is 0.339.

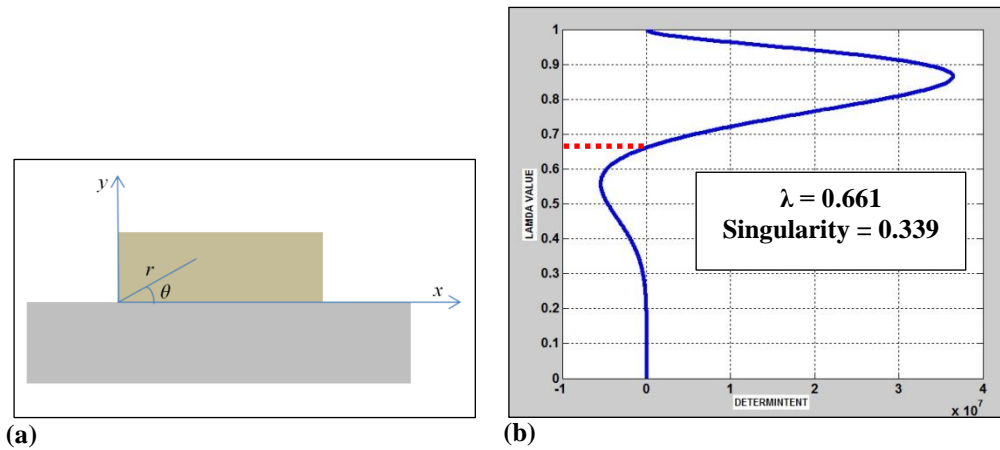


**Figure 3.9: Eigen value determination for stack configuration (a) Co-ordinate system for stack configuration (b) Graph showing obtained value of singularity**

### 3.6.2 Experimental results

Total fringe order over entire model domain is obtained by TFP technique. Using total fringe order data one can get maximum shear stress at each and every pixel over entire model. Figure 3.10 shows the total fringe order plot for linear configuration at 150 N while figure 3.11 shows total fringe order plot for stack configuration at 300 N.

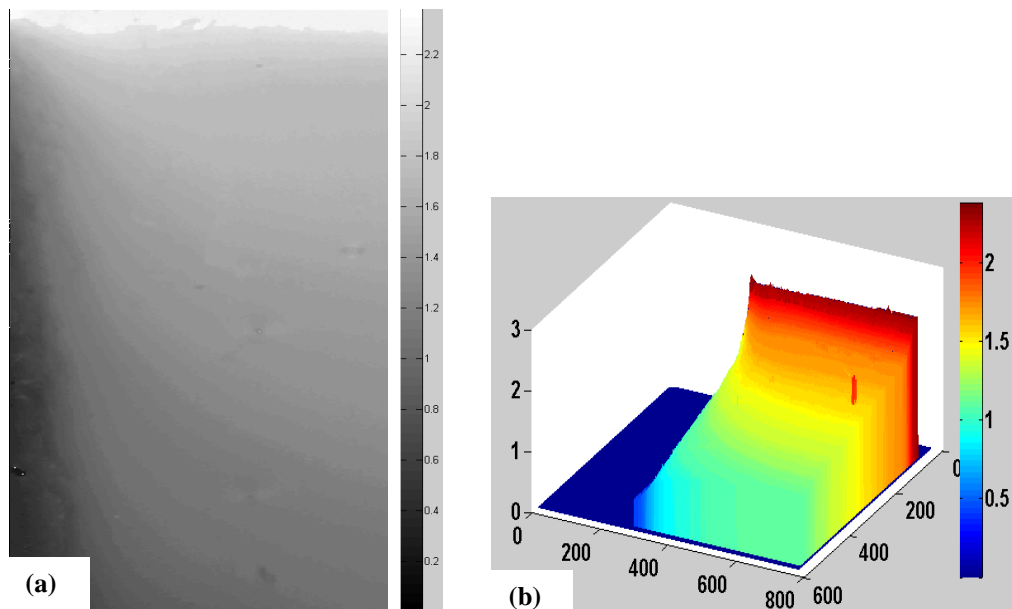


**Figure 3.10: Total fringe order plot for linear configuration (a) Gray scale plot for total fringe order (b) 3D plot for total fringe order**

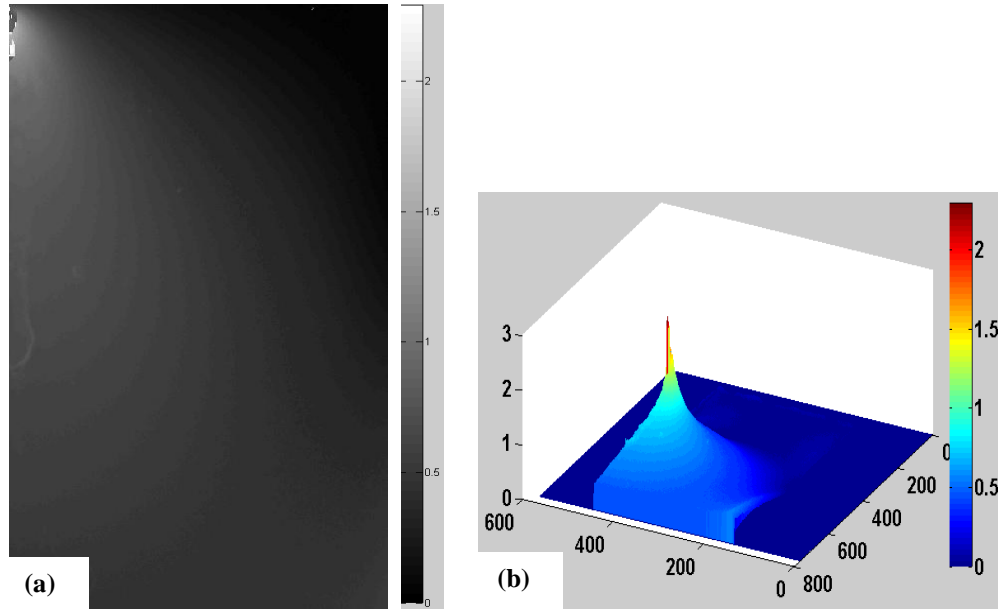


**Figure 3.11: Total fringe order plot for stack configuration (a) Gray scale plot for total fringe order (b) 3D plot for total fringe order**

Fringe order obtained from each pixel data is useful for finding the maximum shear stress over the model domain. In the present study maximum shear stress distribution is plotted along  $0^\circ$  line (along interface) and  $45^\circ$  line across the bimaterial corner. Since there is a practical difficulty in capturing the data points very near to the corner, fringe order data are collected at a radial distance of 3 mm to 12 mm from the corner along  $0^\circ$  line as well as  $45^\circ$  line. From the stress field equations (Eq. 3.1), maximum shear stress will be a function of unknown scale parameter  $k$ , which is obtained from experimentally evaluated maximum shear stress (i.e. for each data points one can get the  $k$  value and best curve can be fit to get the  $k$  value for given bimaterial corner as well as loading condition). The obtained  $k$  value through best curve fit can be used to reconstruct the maximum shear stress distribution along  $0^\circ$  as well as  $45^\circ$ . Figure 3.12 shows  $k$  value determination for linear configuration using  $0^\circ$  data points and obtained value is 0.4296, while using  $45^\circ$  data points it is 0.3925. Similarly for stack configuration obtained value of  $k$  using  $0^\circ$  and  $45^\circ$  data points are 1.025 and 0.935 respectively.

Figure 3.13 shows the experimentally obtained maximum shear stress distribution across the bimaterial corner for both configurations along  $0^\circ$  line as well as  $45^\circ$  line (along with reconstructed maximum shear stress using obtained value of  $k$ ).



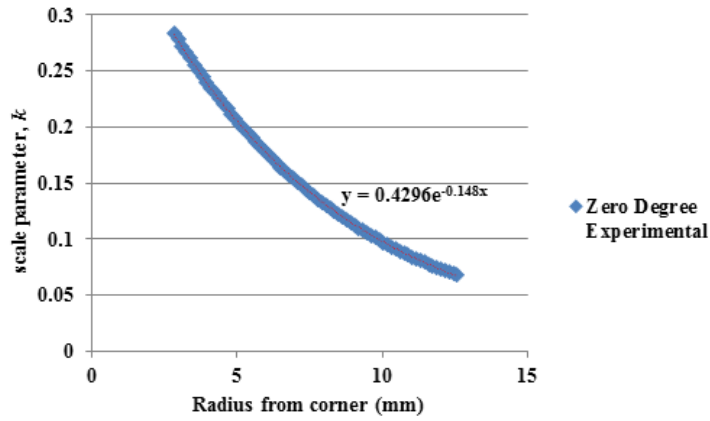
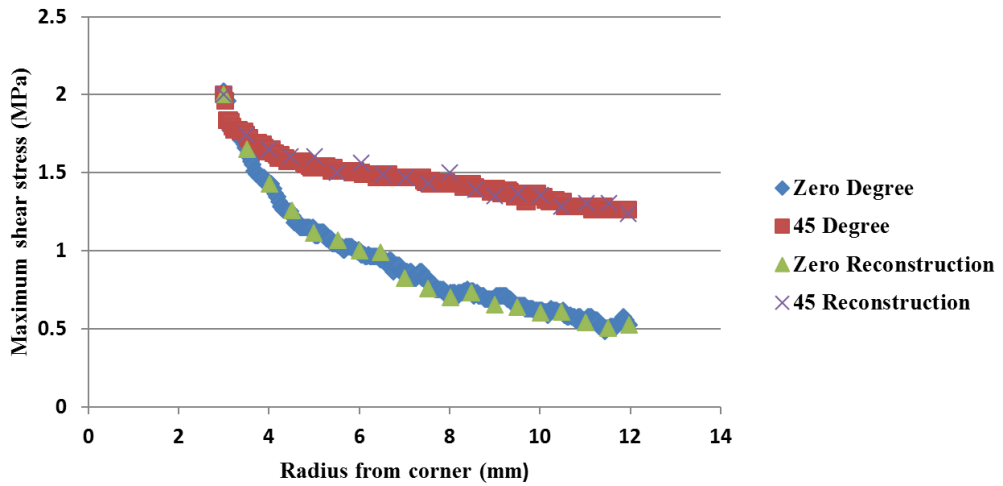
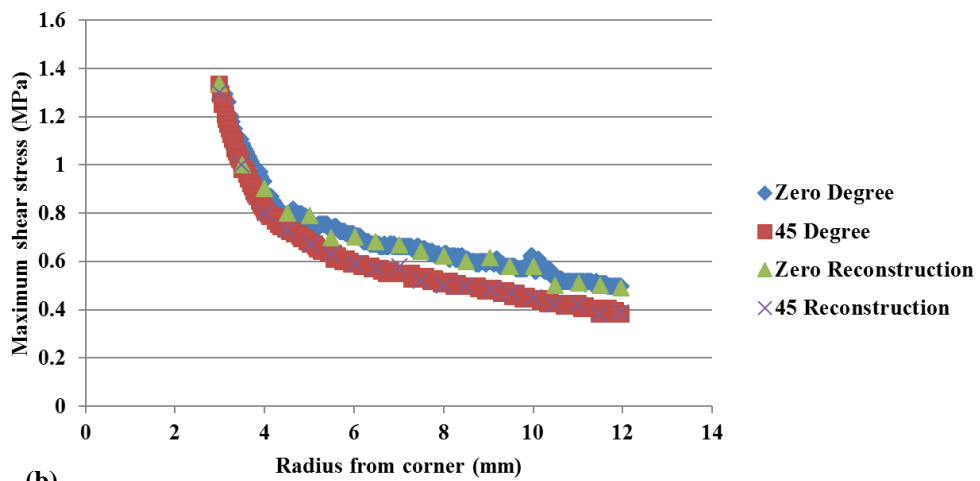


Figure 3.12: Experimental evaluation of  $k$  for linear configuration using  $0^\circ$  data points



(a)



(b)

Figure 3.13: Experimentally obtained maximum shear stress distribution across bimaterial corners (a) Linear configuration (b) Stack configuration

### 3.6.3 Numerical results

Similar to experimental data collection, stress components are evaluated numerically and maximum shear stress is plotted along  $0^\circ$  line as well as  $45^\circ$  line at a distance of 3 mm to 12 mm from bimaterial corner. From the stress field equations (Eq.3.1), maximum shear stress will be a function of unknown scale parameter  $k$ , which can be obtained from numerically evaluated maximum shear stress (i.e. for each data points one can get the  $k$  value and best curve can be fit to get the  $k$  value for given bimaterial corner as well as loading condition). The obtained  $k$  value through best curve fit can be used to reconstruct the maximum shear stress distribution along  $0^\circ$  as well as  $45^\circ$ . Numerically for linear configuration obtained value of  $k$  using  $0^\circ$  and  $45^\circ$  data points are 0.3125 and 0.3611 respectively while for stack configuration the obtained values are 0.996 and 0.954 respectively. Figure 3.14 shows the numerically obtained maximum shear stress distribution across the bimaterial corner for both configurations along  $0^\circ$  line as well as  $45^\circ$  line (along with reconstructed maximum shear stress using obtained value of  $k$ ).

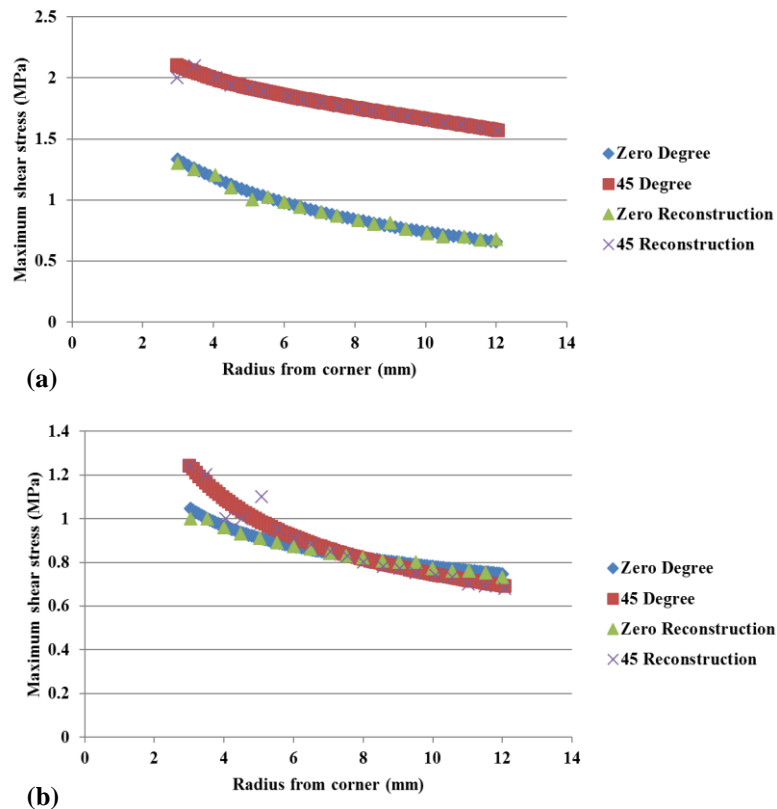


Figure 3.14: Numerically obtained maximum shear stress distribution across bimaterial corners (a) Linear configuration (b) Stack configuration

### 3.6.4 Comparison of experimental and numerical results

As explained earlier the data points collected from  $0^\circ$  as well as  $45^\circ$  are used for maximum shear stress evaluation. The following Figures (3.15 and 3.16) show the comparison of experimental as well as numerical results obtained for both the bimaterial configurations. By seeing at the obtained graphs, there is not much appreciable variation of results but there is appreciable variation in  $45^\circ$  data collection for stack configuration.

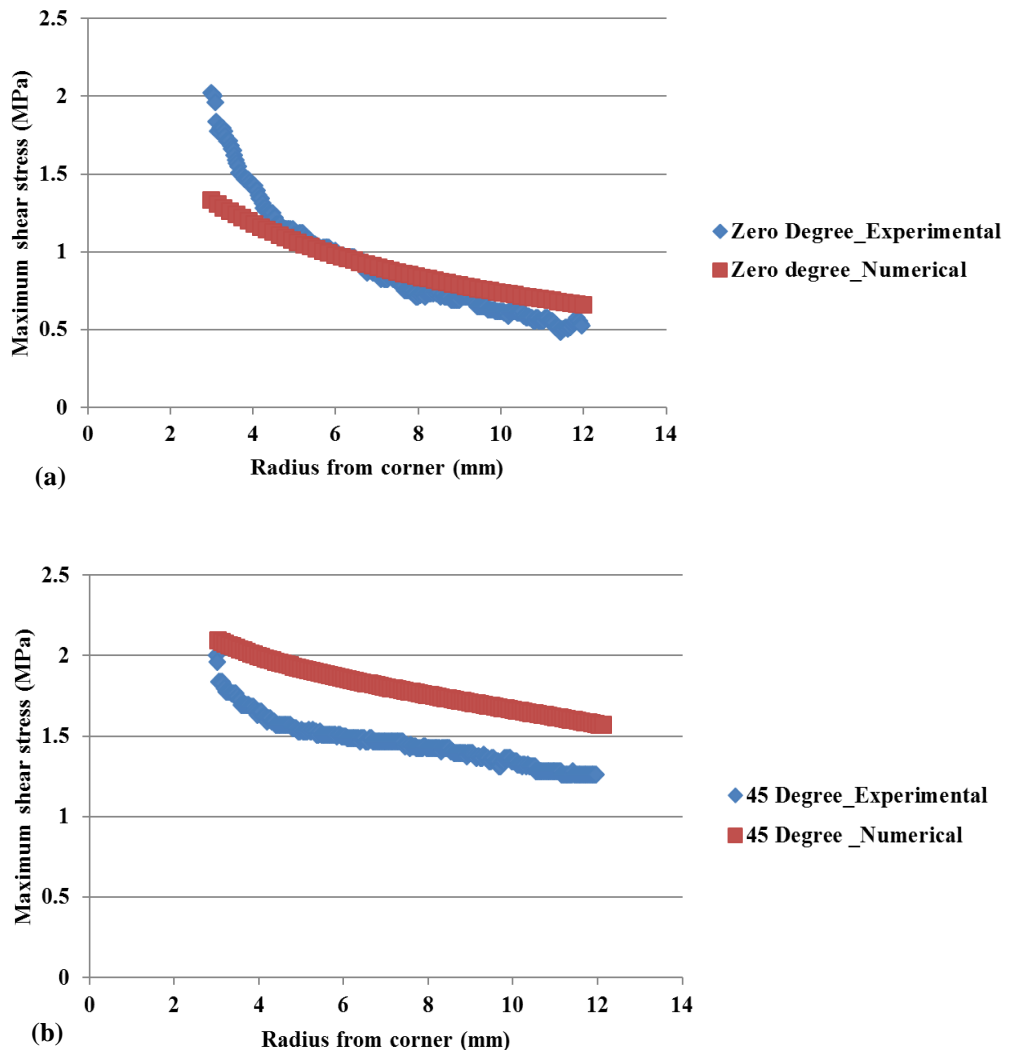


Figure 3.15: Maximum shear stress distribution in linear configuration (a) Zero degree data collection (b) 45 degree data collection

### 3.6.5 Intensity of singularity evaluation

There are various measures to characterize the singular behavior at the corner of bimaterial joints. A stress singularity may develop at the interface corner under an applied loading. Depending on the material elastic properties and the edge geometry the stress singularity may be of the form  $H r^{\lambda-1}$ . The  $H$  field dominates only a local region

near the interface corner of the joint and it is sometimes referred to as a free-edge effect [29]. The intensity  $H$  of the free edge singularity is referred as the free edge intensity factor. The maximum shear stress obtained from the interface data points ( $0^\circ$  line) are related to  $H$  field to get the magnitude of free edge intensity factor. A variation of  $H$  with radial distance from the corner ( $r$ ) has been plotted for  $0^\circ$  data points and has been fitted with a curve. The curve hence obtained is extrapolated to zero radial distance to get  $H$  value of bimaterial corner. The following Figure 3.17 shows the determination of  $H$  for both of the bimaterial configuration under given loading condition. Table 3.1 summarizes the obtained value of free edge intensity factor for both the configuration, experimentally and numerically.

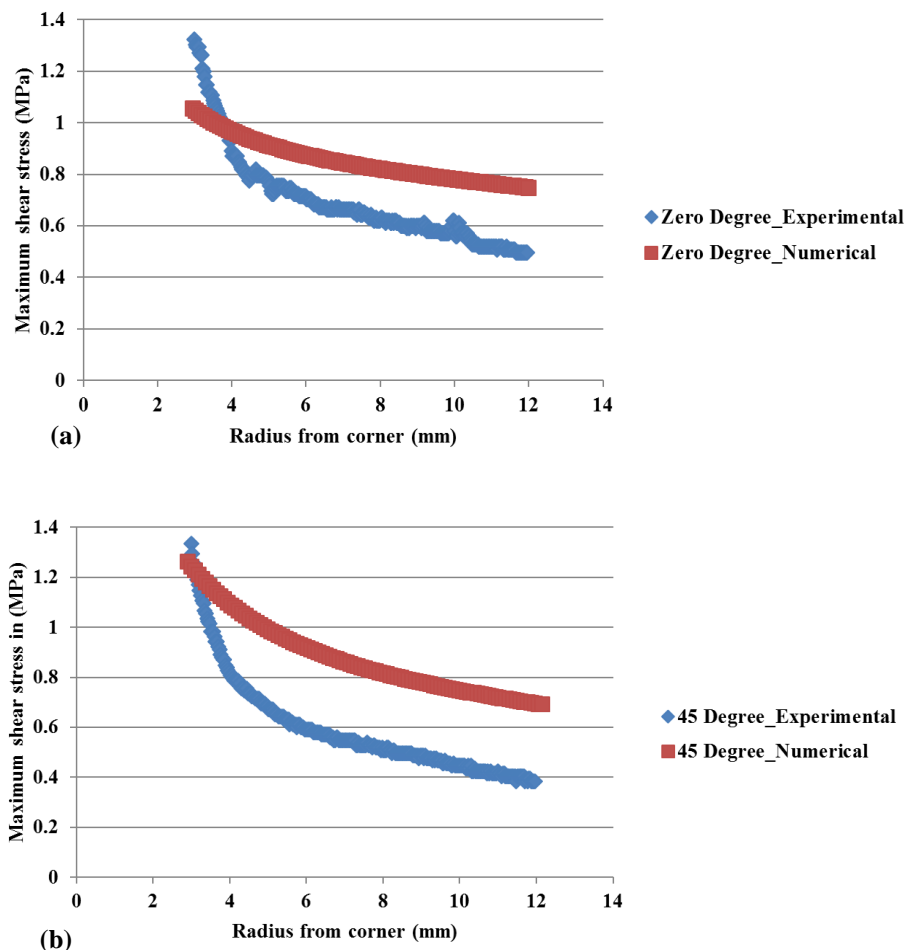


Figure 3.16: Maximum shear stress distribution in stack configuration (a) Zero degree data collection (b) 45 degree data collection

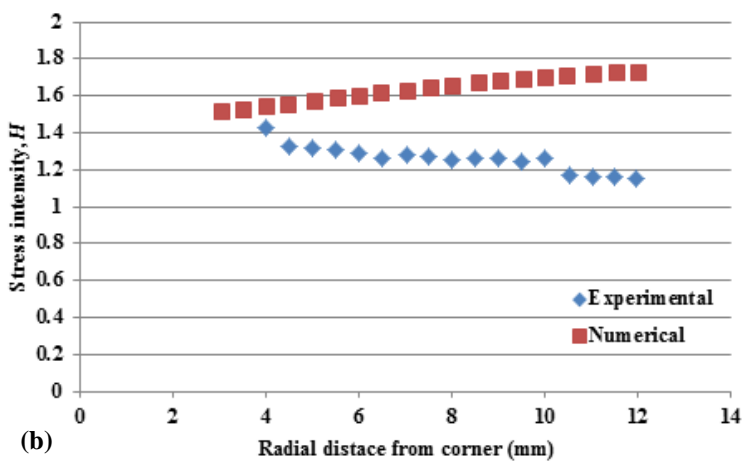
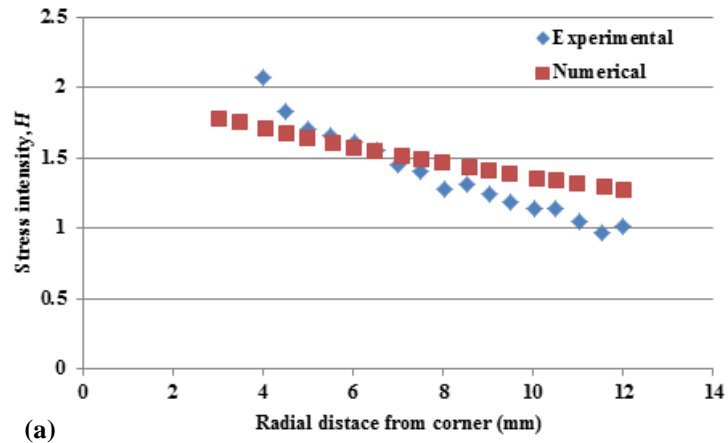


Figure 3.17: Variation of  $H$  with radial distance for bimaterial configuration (a) Linear configuration (b) Stack configuration

Table 3.1:  $H$  value for different bimaterial configurations

Configuration	Experimental ( $H$ )	Numerical ( $H$ )
Linear (MPa(mm) <sup>0.268</sup> )	2.35	1.93
Stack (MPa(mm) <sup>0.339</sup> )	1.56	1.45

### 3.7 Closure

Analytically singularity value of bimaterial configurations are evaluated and it is found that the value lies in between 0 and 1, which depends on material properties forming the corner as well as the geometry of the configurations and is independent of loading conditions. Stack configuration is having higher order of singularity than linear configuration.

Total fringe order over entire model domain is evaluated experimentally by digital photoelasticity involving RTFP technique and the maximum shear stress distribution is plotted along the interface of the bimaterial joint as well as at  $45^\circ$  from the corner of bimaterial joint.

Using the maximum shear stress obtained unknown scale parameter is obtained and then the same stress fields are reconstructed using it. Finally free edge intensity factor is evaluated for both the linear as well as stack configuration under given loading conditions.

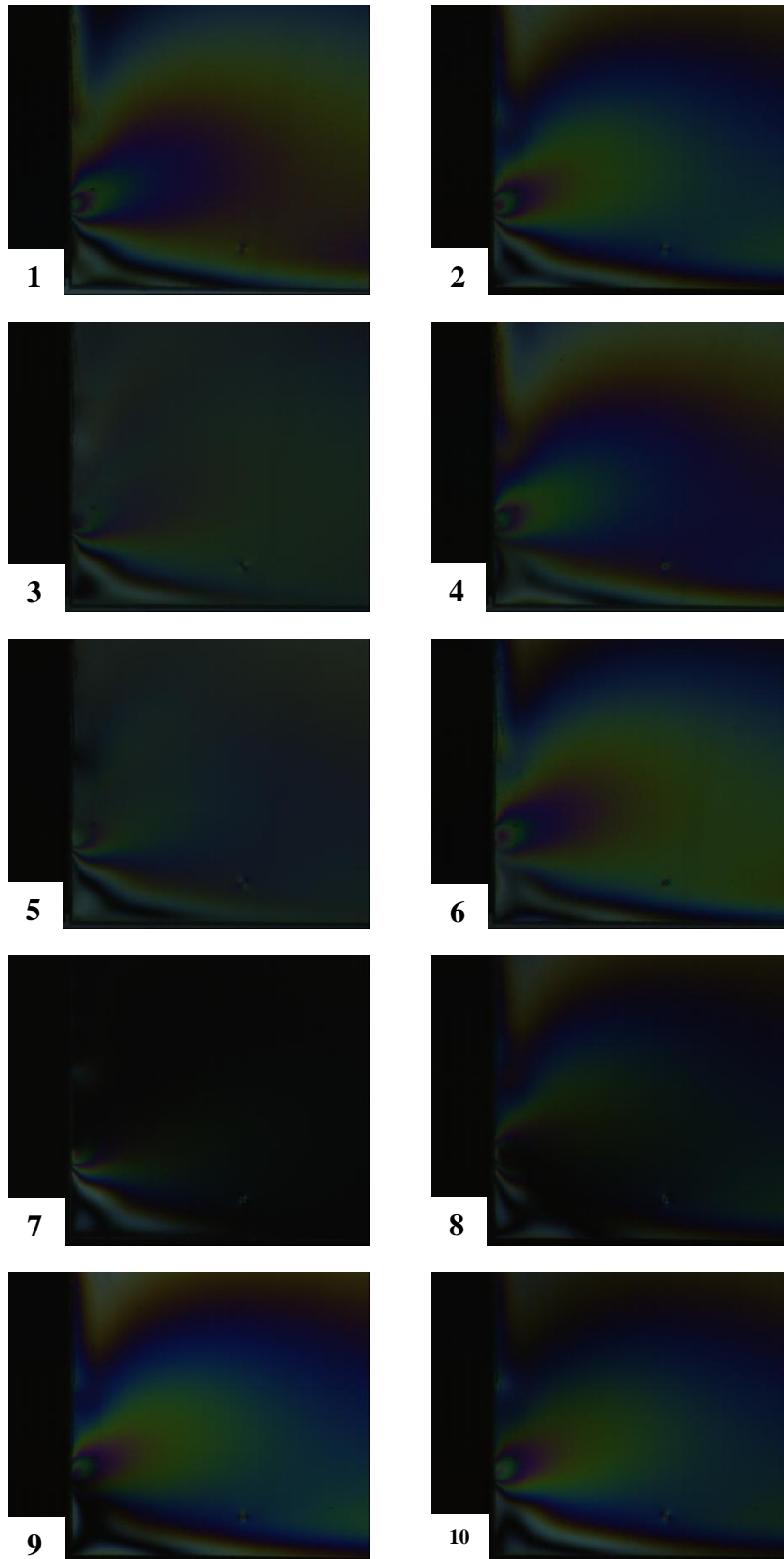
# Chapter 4

## Conclusions and Future Recommendations

In chapter 2, SIF for interfacial cracks in Al / Epoxy bimaterial systems are determined experimentally by digital photoelasticity and numerically by VCCI and  $J$ -integral approach. There is no appreciable difference between numerical results but appreciable variations exist between experimental and numerical results, but order seems to be similar. An improved FE model needs to be developed by incorporating an interfacial layer of adhesive. In chapter 3, analytically singularity value of bimaterial configurations are evaluated and it is found that the value lies in between 0 and 1, which depends on material properties forming the corner as well as the geometry of the configurations and is independent of loading conditions. Stack configuration is having higher order of singularity than linear configuration. Using the obtained order of singularity, scale parameter for bimaterial system is evaluated experimentally and numerically and using this maximum shear stress around bimaterial system is plotted. There exists an appreciable variation in the results obtained by experiments and numerical. Variations between FE and experimental results can be reduced by improving the FE modeling invoking the additional interfacial layer. Concept of non-singular stress terms can be added to the stress fields equations (temperature effect) for further improvement. Generalized SIF for bimaterial corner can be found out by incorporating asymptotic analysis using the concept of angular function approach.

## Appendix A

### Ten-step Images Grabbed at 125 N for Linear Configuration



Figures (1-10) shows the ten images grabbed for experimental analysis



## Appendix B

### Derivation of SIF for an Interfacial Crack

Substituting Eq. 2.6 and Eq. 2.7 into Eq. 2.4 , the energy release rates can be defined as functions of complex SIF,  $K$  .

$$G_I = \frac{c_1 + c_2}{8\pi \cosh(\pi\varepsilon)} \operatorname{Re} \left[ \frac{\Delta^{2i\varepsilon} K^2}{1 + 2i\varepsilon} I_1 + \frac{|K|^2}{1 + 2i\varepsilon} I_2 \right] \quad (\text{B.1})$$

$$G_{II} = \frac{c_1 + c_2}{8\pi \cosh(\pi\varepsilon)} \operatorname{Re} \left[ -\frac{\Delta^{2i\varepsilon} K^2}{1 + 2i\varepsilon} I_1 + \frac{|K|^2}{1 + 2i\varepsilon} I_2 \right] \quad (\text{B.2})$$

$$G_{I-II} = \frac{c_1 + c_2}{4\pi \cosh(\pi\varepsilon)} \operatorname{Im} \left[ \frac{\Delta^{2i\varepsilon} K^2}{1 + 2i\varepsilon} I_1 \right] \quad (\text{B.3})$$

where

$$I_1 = \int_0^{\pi/2} \cos^2 \omega (\sin \omega \cos \omega)^{2i\varepsilon} d\omega \quad (\text{B.4})$$

$$I_2 = \int_0^{\pi/2} \cos^2 \omega (\cos \omega / \sin \omega)^{2i\varepsilon} d\omega = \frac{\pi(1 + 2i\varepsilon)}{4 \cosh(\pi\varepsilon)} \quad (\text{B.5})$$

Dundur (1969) has shown the approximate value of  $I_1$  with an error less than 0.5% is given by,

$$I_1 \approx \frac{\pi}{\cosh(\pi\varepsilon)} \left( \frac{1}{4} - \frac{1}{6} \varepsilon^2 - i \frac{5}{7} \varepsilon \right) \quad (\text{B.6})$$

Substituting Eqs. (B.4) - (B.6) into Eqs. (B.1) - (B.3) and rearranging the equations, the simple relationship between the SIF's and the energy release rates are obtained as,

$$\begin{pmatrix} a_{11}a_{21} + a_{12}^2 & a_{22}a_{21} - a_{12}^2 \\ a_{22}a_{21} - a_{12}^2 & a_{11}a_{21} + a_{12}^2 \end{pmatrix} \begin{pmatrix} K_I^2 \\ K_{II}^2 \end{pmatrix} = \lambda \begin{pmatrix} a_{21}G_I - a_{12}G_{I-II} \\ a_{21}G_{II} + a_{12}G_{I-II} \end{pmatrix} \quad (\text{B.7})$$

where

$$\lambda = \frac{32 \cosh^2(\pi \varepsilon)(1 + 4\varepsilon^2)}{c_1 + c_2}$$

$$a_{11} = (1 + 4\varepsilon^2) + \left(1 - \frac{134}{21} \varepsilon^2\right) \cos[2\varepsilon \ln(\Delta)] + \left(\frac{34}{7} \varepsilon - \frac{4}{3} \varepsilon^3\right) \sin[2\varepsilon \ln(\Delta)]$$

$$a_{12} = 2 \left\{ \left(\frac{34}{7} \varepsilon - \frac{4}{3} \varepsilon^3\right) \cos[2\varepsilon \ln(\Delta)] - \left(1 - \frac{134}{21} \varepsilon^2\right) \sin[2\varepsilon \ln(\Delta)] \right\}$$

$$a_{22} = (1 + 4\varepsilon^2) - \left(1 - \frac{134}{21} \varepsilon^2\right) \cos[2\varepsilon \ln(\Delta)] - \left(\frac{34}{7} \varepsilon - \frac{4}{3} \varepsilon^3\right) \sin[2\varepsilon \ln(\Delta)]$$

$$a_{21} = 4 \left\{ \left(1 - \frac{134}{21} \varepsilon^2\right) \cos[2\varepsilon \ln(\Delta)] + \left(\frac{34}{7} \varepsilon - \frac{4}{3} \varepsilon^3\right) \sin[2\varepsilon \ln(\Delta)] \right\}.$$

# References

1. P. S. Theocaris, The order of singularity at a multi-wedge corner of a composite plate, *Int. J. Eng. Sc.*, vol. 12, 1974, pp. 107-120.
2. K. M. Lim, K. H. Lee, A. A. O. Tay, and W. A. Zhou, New variable-order of singular boundary element for stress analysis, *Int. J. Numer. Meth. Eng.*, vol. 55, 2002, pp. 293-316.
3. P. E. Garrou, E. J Vardaman and P. D. Franzon, Through silicon via technology: The ultimate market for 3D interconnect, *Tech search international*, January 2008.
4. Williams, M. L. Stresses around a fault or a crack in dissimilar media. *Bull. Seismol.soc. America*, 1959, vol. 49, pp. 199-204.
5. Ramesh, K., Gupta, S., and Kelkar, A. A. Evaluation of stress field parameters in fracture mechanics by photoelasticity-revisited. *Eng Fracture Mechanics*, 1997, 56(1), 25–45.
6. Rice, J. R. Elastic fracture mechanics concepts for interfacial cracks. *Tran. ASME, J. Appl. Mechanics*, vol. 55, 1988, pp. 98-103.
7. Deng, X. General crack tip fields for stationary and steadily growing interface cracks in anisotropic bimetals. *Trans. ASME, J. Appl. Mechanics*, vol. 60, 1993, pp. 183-189.
8. Ravichandran, M., and Ramesh, K., Evaluation of stress field parameters for an interface crack in a bimaterial by digital photoelasticity. *J. Strain Anal. Eng. Des.* vol. 40, 2005, pp. 327-343.
9. *Hand book of experimental solid mechanics*, (Ed. N. N. Sharpe), 2008, Springer, New York.
10. M. Ramji, Whole field stress separation in digital photoelasticity by shear difference – issues, implementation and application, PhD Thesis, 2007, IIT Madras.
11. A.S Voloshin, and C.P. Burger, Half fringe photoelasticity – a new approach to whole field stress analysis. *Experimental Mechanics*, vol. 23(9), 1983, pp. 304–314.

12. Sai Prasad, V., K.R. Madhu and K. Ramesh (2004) Towards effective phase unwrapping in digital photoelasticity. *Optics and Lasers in Engineering*, 42(4):421-436.
13. Siegmann, P., D. Backman and E.A. Patterson (2005) A robust approach to demodulating and unwrapping phase-stepped photoelastic data. *Experimental Mechanics*, 45(3):278-289.
14. K Ramesh, S. S. Deshmukh, Three fringe photoelasticity-use of colour image processing hardware to automate ordering of isochromatics. *Strain*, vol. 32(3), pp. 79-86.
15. K. R. Madhu, R. G. R Prasath, K. Ramesh, Colour adaptation in three fringe photoelasticity, *Experimental mechanics*, vol. 47, 2007, pp. 271-276.
16. Lu, H. and Chiang, F. P., Photoelastic determination of SIF of an interfacial crack in a bimaterial, *Tran. ASME, J. Appl. Mechanics*, vol. 60, 1993, pp. 93-100.
17. Soh, A. K. An improved photoelastic technique for determining the mixed mode SIF's for interfacial cracks in a bimaterial. *Composites Sci. Technol.*, vol. 59, 1999, pp. 1033-1039.
18. Ramji and Ramesh K, Whole field evaluation of stress field components in digital photoelasticity – issues, implementation and application, *Opt. lasers in engineering*, vol. 46, 2008, pp. 257-251.
19. Williams, M. L., The stress singularities resulting from various boundary conditions in angular corners of plates in extension, *Trans. ASME, J. Appl. Mech.*, vol. 19, 1952, pp. 526-529.
20. Bogy, D.B., Edge-bonded dissimilar orthogonal elastic wedges under normal and shear loading, *Trans. ASME, J. Appl. Mech.*, vol. 35, 1968, pp. 460-466.
21. Munz, D. and Yang, Y. Y., Stress singularities at the interface in bonded dissimilar materials under mechanical and thermal loading, *Trans. ASME, J. Appl. Mech.*, Vol.59, 1992, pp. 857-861.
22. Liton Kumar, Arai and Tsuchida, An analysis on singular fields around an interface edge of ceramic/metal joints using Moiré interferometry technique, *JSME journal*, vol. 48, 2005, pp.240-245.

23. Seweryn A, Molski K. Elastic stress singularities and corresponding generalized stress intensity factors for angular corners under various boundary conditions. *Eng. Fracture mech.* vol. 55, 1996, pp. 529-556.
24. Yaping Luo and Ganesh Subbarayan, A study of multiple singularities in multi-material wedges and their use in analysis of microelectronic interconnect structures, *Engineering fracture mechanics*, vol. 74, 2007, pp. 416-430.
25. Dattaguru. B, Venkatesha. K. S, Ramamurthy. T. S and Buchholz. F. G, FE estimates of strain energy release rate components at the tip of an interface crack under mode I loading, *Eng. Fracture mechanics*, vol. 49, 1994, pp. 451-463.
26. Chow, W. T, Atluri, S. N, FE calculation of SIF's for interfacial crack using virtual crack closure integral. *Computational mechanics*, vol. 16, 1995, pp. 417-425.
27. M. Ramji and Prasath RGR, Sensitivity of isoclinic data using various phase shifting techniques in digital photoelasticity towards generalized error sources, *Optics and Lasers in Engineering*, Vol. 49, No. 9-10, 2011, 1153-1167.
28. Ramesh K, *Digital Photoelasticity: Advanced techniques and applications*. Springer- Verlag, Berlin, Germany, 2000.
29. Qian Z, Akisanya A R, An investigation of stress singularity near the free edge of scarf joints, *Eur. J. Mech. A / solids*, 18, pp.443-463.

# List of the Papers Submitted on the Basis of this Thesis

Rahul N Pai, M Ramji, "*Experimental and Numerical Evaluation of SIF for a Bimaterial Interface Crack subjected to Pure Bending*", International Conference on Structural Stability and Dynamics -12, January 4-6, 2012, Jaipur.

\*\*\*\*\*